Numerical solution of coupled steady-state hot-phonon–hot-electron Boltzmann equations in InP

J. C. Vaissiere and J. P. Nougier
Centre d'Electronique de Montpellier, Université Montpellier II, 34095 Montpellier CEDEX 5, France

M. Fadel
Faculté des Sciences d'Agadir, Agadir, Morocco

L. Hlou
Faculté des Sciences de Kénitra, Kénitra, Morocco

P. Kocevar
Institut für Theoretische Physik, Universität Graz, Universitätsplatz 5, A-8010 Graz, Austria
(Received 10 February 1992)

A matrix method for the numerical determination of steady-state hot-phonon and nondegenerate hot-electron distribution functions is presented. The coupled Boltzmann equations for the longitudinal-optical phonons and for the electrons, in the Γ and L valleys of III-V semiconductor compounds, are iteratively solved with high accuracy under typical hot-electron conditions. The phonon distribution is shown to be significantly disturbed from thermal equilibrium. In turn, nonequilibrium phonons induce a substantial disturbance of the hot-electron distribution. Computations are performed for InP at 300 K, taking into account all relevant scattering mechanisms. It turns out that the electron transport parameters are strongly affected in the field range from 0 to 10 kV/cm: the drift velocity is increased by about 42% at 2 kV/cm and the Ohmic mobility by 37%. These effects are shown to be due to the drag and reduced cooling of the carriers by the nonequilibrium LO phonons.

I. INTRODUCTION

When calculating hot-carrier transport, one usually solves the Boltzmann equation, assuming that the reservoir of phonons is in thermal equilibrium. However, the phonon distribution may be significantly disturbed, when the carrier scattering rate of a given type of phonon is comparable to the nonelectronic thermalization rate of these phonons.[1] In the case of acoustic and piezoelectric phonons, this disturbance occurs at low temperature.[1,2]

Conversely, optical phonons may be strongly disturbed even at room temperature, as observed by picosecond laser-pulsed experiments.[3–5] In hot-electron transport, the emission of longitudinal-optical (LO) phonons is the main energy-relaxation mechanism of charge carriers in III-V semiconductor compounds at intermediate fields, that is, at fields large enough for electrons to gain, during a mean free flight, an energy higher than the energy $\hbar\omega_{\mathrm{LO}}$ of a LO phonon and lower than the energy gap Δ between the Γ-valley minimum and the next higher (generally the L) -band minima. Therefore, the electric-field range in which we are interested in for studying phonon disturbances and their effect on the electron dynamics is such that only the two lowest types of valleys are involved.

In this paper we present a method for numerically solving the coupled hot-phonon–hot-electron Boltzmann equations for the steady state. This will allow us to study the disturbance of the distribution function of the LO phonons from equilibrium, induced by the hot carriers, and the ensuing modifications of the distribution of the hot electrons due to the amplification and displacement of the phonon distribution. We will then be able to study the corresponding modification of electronic transport parameters. These results will confirm and complement the earlier carrier-temperature or Monte Carlo approach for the investigation of nonequilibrium LO-phonon effects on non-Ohmic transport in polar semiconductors.[2,6–8]

In Sec. II, the numerical method will be described. The expression of the Boltzmann equation for the phonons and for the electrons will be given in Secs. III and IV, and the results obtained for InP will be described in Sec. V.

II. METHOD OF SOLUTION

In this section, we shall give the method used for determining the steady state by solving the coupled Boltzmann equations for nondegenerate hot electrons and hot phonons, in homogeneous III-V semiconductor compounds, for a uniform external electric field **E**.

The evolution of the phonon distribution function $N(\mathbf{q},t)$ is obtained from the solution of the Boltzmann equation

$$\frac{\partial N(\mathbf{q},t)}{\partial t}=\left\{\frac{\partial N(\mathbf{q},t)}{\partial t}\right\}_{\mathrm{elec}}+\left\{\frac{\partial N(\mathbf{q},t)}{\partial t}\right\}_{\mathrm{latt}}, \tag{1}$$

where the two terms on the right-hand side are related to the variations of $N(\mathbf{q},t)$ produced by electron-phonon and by phonon-phonon collision processes. We shall take

into account only the LO phonons, since disturbances of other phonon branches will be negligible in the high-temperature regime of our following applications.[1,8] One may then write

$$\left[\frac{\partial N(\mathbf{q},t)}{\partial t}\right]_{\text{elec}} = \hat{C}_{\text{ph}} N(\mathbf{q},t) - \hat{D}_{\text{ph}} N(\mathbf{q},t) , \tag{2}$$

where $\hat{C}_{\text{ph}}$ and $\hat{D}_{\text{ph}}$ are gain and loss operators, respectively, related to emission and absorption of phonons by electrons. The expressions for these operators will be given below, in Sec. III. Their important feature is that they depend on the electron distribution function $f(\mathbf{k},t)$.

The lattice scattering term in Eq. (1) can be simply described through a relaxation time τ_L, which will be given in Sec. III below:

$$\left[\frac{\partial N(\mathbf{q},t)}{\partial t}\right]_{\text{latt}} = -\frac{N(\mathbf{q},t)-N_L}{\tau_L} , \tag{3}$$

where N_L is the thermal-equilibrium Bose-Einstein distribution. Finally, Eqs. (1), (2), and (3) lead to

$$\frac{\partial N(\mathbf{q},t)}{\partial t} = \hat{C}_{\text{ph}} N(\mathbf{q},t) - \hat{D}_{\text{ph}} N(\mathbf{q},t) - \frac{N(\mathbf{q},t)-N_L}{\tau_L} . \tag{4}$$

As concerns the electrons, we are interested in GaAs-like III-V semiconductor compounds, where three groups of valleys are involved: the Γ, L, and X valleys. However, as explained in the Introduction, the electric fields of interest for the present study are such that only two groups of valleys are involved, namely the Γ and the L valleys. The Boltzmann equations for this two-band model are then

$$\frac{\partial f_1(\mathbf{k},t)}{\partial t} = -\frac{e\mathbf{E}}{\hbar}\nabla_k f_1(\mathbf{k},t) + \hat{C}_{11} f_1(\mathbf{k},t) + \hat{C}_{12} f_2(\mathbf{k},t) - \frac{f_1(\mathbf{k},t)}{\tau_1(\mathbf{k})} , \tag{5}$$

$$\frac{\partial f_2(\mathbf{k},t)}{\partial t} = -\frac{e\mathbf{E}}{\hbar}\nabla_k f_2(\mathbf{k},t) + \hat{C}_{22} f_2(\mathbf{k},t) + \hat{C}_{21} f_1(\mathbf{k},t) - \frac{f_2(\mathbf{k},t)}{\tau_2(\mathbf{k})} , \tag{6}$$

where the subscripts 1 and 2 stand for Γ and L, respectively. $\hat{C}_{11}$ and $\hat{C}_{22}$ are the "entrance terms" for intravalley scattering, corresponding to the sum of the scattering from any state $\mathbf{k}'$ of a given valley (Γ or L) to the state $\mathbf{k}$ of the same valley. $\hat{C}_{12}$ and $\hat{C}_{21}$ describe intervalley scattering; they correspond to the sum of the scattering from any state $\mathbf{k}'$ of a given valley (Γ or L) to the state $\mathbf{k}$ of the other valley (L or Γ). $1/\tau_1(\mathbf{k})$ is the "exit term from the valley Γ," corresponding to the sum of the scatterings from a given state $\mathbf{k}$ of the valley Γ, to any state $\mathbf{k}'$ of any valley (Γ or L), and $1/\tau_2(\mathbf{k})$ is the "exit term from the valley L." These expressions will be detailed in Sec. IV.

The operators $\hat{C}_{jj}$ depend on $N(\mathbf{q},t)$, which is assumed to be constant, when hot LO phonons are neglected, but which is not constant in this study. We should then solve the system of nonlinear coupled equations (4)–(6), with the unknowns $N(\mathbf{q},t)$, $f_1(\mathbf{k},t)$, and $f_2(\mathbf{k},t)$. We are interested in the steady-state regime, given by

$$\hat{C}_{\text{ph}} N(\mathbf{q}) - \hat{D}_{\text{ph}} N(\mathbf{q}) - \frac{N(\mathbf{q})-N_L}{\tau_L} = 0 , \tag{7}$$

$$-\frac{e\mathbf{E}}{\hbar}\nabla_k f_1(\mathbf{k}) + \hat{C}_{11} f_1(\mathbf{k}) + \hat{C}_{12} f_2(\mathbf{k}) - \frac{f_1(\mathbf{k})}{\tau_1(\mathbf{k})} = 0 , \tag{8}$$

$$-\frac{e\mathbf{E}}{\hbar}\nabla_k f_2(\mathbf{k}) + \hat{C}_{22} f_2(\mathbf{k}) + \hat{C}_{21} f_1(\mathbf{k}) - \frac{f_2(\mathbf{k})}{\tau_2(\mathbf{k})} = 0 . \tag{9}$$

In the following, this system will be solved by extending the matrix method developed by Aubert and two of the present authors[9] to the non-equilibrium-phonon case. Since this system is nonlinear, only an iterative method can be used, consisting in the following steps.

(i) The phonon distribution is first taken as being the Bose-Einstein thermal-equilibrium distribution $N(\mathbf{q}) = N^{(0)}(\mathbf{q}) = N_{\text{LO}}$. Inserting N_{LO} into Eqs. (8) and (9), one gets, after discretization, a linear homogeneous system [since the derivatives involved in ∇_k and the integrals involved in $\hat{C}_{ij}$ can be expressed as linear forms of $f_i(\mathbf{k})$]. This system is solved using a least-square method suited for overdetermined systems.[9] One then gets a first estimate of the $f_i(\mathbf{k})$, labeled $f_i^{(0)}(\mathbf{k})$, which is the electron distribution function one would obtain neglecting hot-phonon effects, i.e., the hot-carrier distribution function usually studied. Note that, since the system of Eqs. (8) and (9) is homogeneous, one gets an infinite set of proportional values of $f_1(\mathbf{k})$ and $f_2(\mathbf{k})$. The correct values are obtained by normalizing $f_1(\mathbf{k})+f_2(\mathbf{k})$ to the total carrier density N_c, set equal to N_D for uncompensated and nondegenerate material at room temperature.

(ii) The $f_i^{(0)}(\mathbf{k})$ are now carried into Eq. (7), which then becomes a linear equation, which is solved using the above technique, giving a phonon distribution $N^{(1)}(\mathbf{q})$.

(iii) $N^{(1)}(\mathbf{q})$ is carried into Eqs. (8) and (9), giving distributions $f_i^{(1)}(\mathbf{k})$, then a new distribution $N^{(2)}(\mathbf{q})$ is found from Eq. (7), and this process is continued until convergence is reached, when two successive electron, as well as phonon, distributions agree within the desired accuracy.

III. THE PHONON BOLTZMANN EQUATION

A. Lattice relaxation

In Eq. (7), N_L is the Bose-Einstein thermal-equilibrium distribution

$$N_L = \left[\exp\left[\frac{\hbar\omega_{\text{LO}}}{k_B T_L}\right] - 1\right]^{-1} , \tag{10}$$

where $\hbar\omega_{\text{LO}}$ is the energy of the LO phonon, k_B is the Boltzmann constant, and T_L is the lattice temperature.

The relaxation time τ_L for LO-phonon thermalization is given by[10]

$$\tau_L = \frac{\tau_0}{1+\left[\exp\left[\frac{0.65\hbar\omega_{\mathrm{LO}}}{k_B T_L}\right]-1\right]^{-1}+\left[\exp\left[\frac{0.35\hbar\omega_{\mathrm{LO}}}{k_B T_L}\right]-1\right]^{-1}} , \tag{11}$$

where τ_0 has been found experimentally to lie in the range 8–20 ps in GaAs.[5,8,11–13]

B. Phonon-emission operator $\hat{C}_{\mathrm{ph}}$

The rate of LO phonons generated in the state $\mathbf{q}$ by electrons, initially in state $\mathbf{k}$, emitting a LO phonon and ending up in the state $\mathbf{k}-\mathbf{q}$, is written as

$$\hat{C}_{\mathrm{ph}}N(\mathbf{q}) = \frac{2\Omega}{8\pi^3}\int_{\mathbf{k}} P_{\mathrm{po,emi}}(\mathbf{k},\mathbf{k}'=\mathbf{k}-\mathbf{q}) f(\mathbf{k}) d^3k ,$$

so that, neglecting free-carrier screening of the polar-optical coupling,

$$\hat{C}_{\mathrm{ph}}N(\mathbf{q}) = \frac{[N(\mathbf{q})+1]}{q^2} 2C_{\mathrm{po}} \times \int_{\mathbf{k}} G(\mathbf{k},\mathbf{k}-\mathbf{q}) f(\mathbf{k}) \times \delta\{\varepsilon(\mathbf{k}-\mathbf{q})-[\varepsilon(\mathbf{k})-\hbar\omega_{\mathrm{LO}}]\} d^3k , \tag{12a}$$

with

$$C_{\mathrm{po}} = \frac{e^2\hbar\omega_{\mathrm{LO}}}{\pi^2\hbar\varepsilon_0}\left[\frac{1}{\varepsilon_\infty}-\frac{1}{\varepsilon_r}\right] . \tag{12b}$$

In Eq. (12a), $\varepsilon(\mathbf{k})$ and $\varepsilon(\mathbf{k}-\mathbf{q})$ are the energies of the electron before and after a phonon emission, and $\hbar\omega_{\mathrm{LO}}$ is assumed to be independent of $\mathbf{q}$. Furthermore,

$$G(\mathbf{k},\mathbf{k}-\mathbf{q}) = G(\mathbf{k}-\mathbf{q},\mathbf{k}) = [a(\mathbf{k})a(\mathbf{k}-\mathbf{q})+c(\mathbf{k})c(\mathbf{k}-\mathbf{q})\cos\beta]^2 , \tag{12c}$$

with

$$a(\mathbf{k}) = \left[\frac{1+\alpha^*\varepsilon(\mathbf{k})}{1+2\alpha^*\varepsilon(\mathbf{k})}\right]^{1/2}$$

and

$$c(\mathbf{k}) = \left[\frac{\alpha^*\varepsilon(\mathbf{k})}{1+2\alpha^*\varepsilon(\mathbf{k})}\right]^{1/2} , \tag{12d}$$

where β is the angle between the vectors $\mathbf{k}$ and $\mathbf{k}-\mathbf{q}$ [in shortened notation, $\beta=(\mathbf{k},\mathbf{k}-\mathbf{q})$], α^* is the nonparabolicity factor of the bands, and ε_∞ and ε_r are the relative high-frequency and static dielectric constants.

It is much easier to compute the integral (12a) using polar coordinates with a polar axis along $\mathbf{q}$. Then (see Fig. 1 and Appendix A) $\mathbf{k}=\{k,\zeta,u\}$, and in this system

$$f(\mathbf{k}) = f(k,\zeta,u) ,$$
$$\varepsilon(\mathbf{k}-\mathbf{q})-[\varepsilon(\mathbf{k})-\hbar\omega_{\mathrm{LO}}] = H_c(k,q,\zeta) , \tag{13}$$
$$G(\mathbf{k}-\mathbf{q},\mathbf{k}) = G(k,q,\zeta) .$$

The calculation is detailed in Appendix A. Equation (12a) can be written as

$$\hat{C}_{\mathrm{ph}}N(\mathbf{q}) = \frac{[N(\mathbf{q})+1]}{q^3} 2A_{\mathrm{po}} \times \int_{k=k_{\mathrm{min}C}}^{k_{\mathrm{max}}} P_c(k)dk \int_{u=0}^{\pi} f[k,\theta_0(u)]du , \tag{14}$$

with

$$A_{\mathrm{po}} = \frac{e^2\hbar\omega_{\mathrm{LO}}m^*}{\pi^2\hbar^3\varepsilon_0}\left[\frac{1}{\varepsilon_\infty}-\frac{1}{\varepsilon_r}\right] , \tag{15}$$

$$P_c(k) = \frac{k}{(1+2\alpha^*\varepsilon)}[(1+\alpha^*\varepsilon)^{1/2}(1+\alpha^*\varepsilon')^{1/2} + \alpha^*(\varepsilon\varepsilon')^{1/2}\cos\beta_0]^2 , \tag{16}$$

$$\varepsilon' = \varepsilon-\hbar\omega_{\mathrm{LO}} . \tag{17}$$

As shown in Eqs. (A14), $k_{\mathrm{min}C}$ is a function of q. This function also depends on the effective mass m^* and on the nonparabolicity factor α^*, that is on the valley in which the process is studied. Figure 2 shows, in indium phosphide, the variations of $k_{\mathrm{min}C}$ vs q, for emission of phonons, in the valleys Γ and L [circles ($\circ$) and horizontal crosses (+)]. In practice k_{max} is chosen such that $f(k_{\mathrm{max}})$ is negligible; typically, $k_{\mathrm{max}}\approx 1.6\times10^9$ m^{-1} (dashed line in Fig. 2). From Eqs. (A13) and (A20),

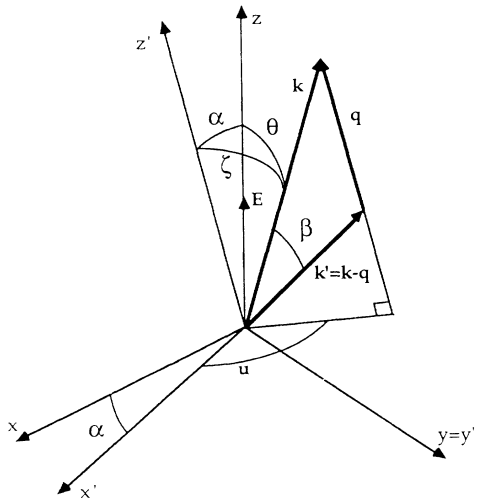

FIG. 1. The electron distribution function $f(\mathbf{k})=f(k,\theta)$ is computed in the coordinate system $\{x,y,z\}$ with $\mathbf{z}$ along the electric field $\mathbf{E}$, $k=|\mathbf{k}|$, and $\theta=(\mathbf{E},\mathbf{k})$. The phonon distribution is $N(\mathbf{q})=N(q,\alpha)$ with $q=|\mathbf{q}|$ and $\alpha=(\mathbf{E},\mathbf{q})$. The integrals involved in the phonon Boltzmann equation are computed in the coordinate system $\{x',y',z'\}$ with $\mathbf{z}'$ along $\mathbf{q}$.

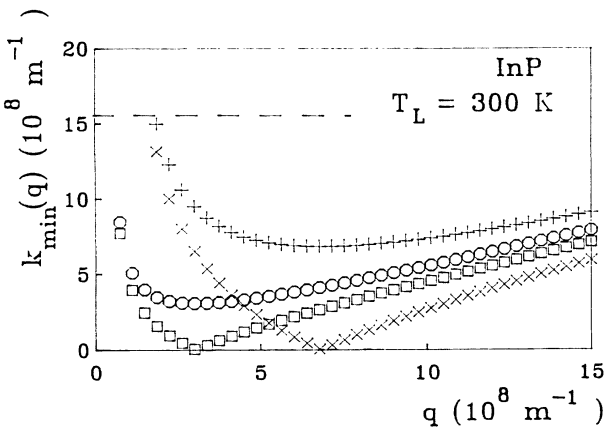

FIG. 2. Variation of $k_{min}=k_{minC}$ and of $k_{min}=k_{minD}$ vs q, for emission of LO phonons in the Γ valley (circles ○, $k_{min}=k_{minC}$), absorption of LO phonons in the Γ valley (squares □, $k_{min}=k_{minD}$), emission of LO phonons in the L valley (crosses +, $k_{min}=k_{minC}$), and absorption of LO phonons in the L valley (oblique crosses ×, $k_{min}=k_{minD}$). The dashed line corresponds to the value of k_{max}.

$$\cos\beta_{0C}=\frac{k-qs_{0C}}{(k^2+q^2-2kqs_{0C})^{1/2}}\ , \tag{18}$$

with

$$s_{0C}=\frac{q}{2k}+\frac{m^*\omega_{LO}}{\hbar kq}[1+\alpha^*(\varepsilon'+\varepsilon)]\ ,$$
$$\varepsilon'=\varepsilon-\hbar\omega_{LO}\ , \tag{19}$$

and, from Eqs. (A22) and (A21),

$$\cos[\theta_{0C}(u)]=s_{0C}\cos\alpha-(1-s_{0C}^2)^{1/2}\sin\alpha\cos u\ . \tag{20}$$

The double integral in Eq. (14) has no analytical solution, and the electron distribution function is tabulated at the k_i and θ_j values of the mesh in $\{\mathbf{k}\}$ space, through the numerical solution of the electron Boltzmann equation.

Equation (14) holds for $q_{min}\le q\le q_{max}$. As discussed in Appendix A,

$$q_{min}=k(\varepsilon_{max})-k(\varepsilon_{max}-\hbar\omega_{LO})\ ,$$
$$q_{max}=k(\varepsilon_{max})+k(\varepsilon_{max}-\hbar\omega_{LO})\ , \tag{21}$$

where, as shown in Fig. 2, q_{min} also depends on the valley through m^* and α^*. In practice, the value q_{max} is very large; we limited ourselves to $q_{max}=1.5\times10^9\ m^{-1}$.

C. Phonon-absorption operator $\hat{D}_{ph}$

The rate of destruction of LO phonons in the state $\mathbf{q}$ by electrons, initially in states $\mathbf{k}$, absorbing an LO phonon and ending up in states $\mathbf{k}+\mathbf{q}$, is written as

$$\hat{D}_{ph}N(\mathbf{q},t)=\frac{2\Omega}{8\pi^3}\int_{\mathbf{k}}P_{po,abs}(\mathbf{k},\mathbf{k}'=\mathbf{k}+\mathbf{q})f(\mathbf{k})d^3k\ , \tag{22}$$

so that

$$\hat{D}_{ph}N(\mathbf{q},t)=\frac{N(\mathbf{q})}{q^2}2C_{po}\times\int_{\mathbf{k}}G(\mathbf{k},\mathbf{k}+\mathbf{q})f(\mathbf{k})\times\delta\{\varepsilon(\mathbf{k}+\mathbf{q})-[\varepsilon(\mathbf{k})+\hbar\omega_{LO}]\}d^3k\ , \tag{23}$$

where C_{po} is given by Eq. (12b). Using the same procedure as for computing $\hat{C}_{ph}$, one gets, in analogy with Eqs. (14)–(21),

$$\hat{D}_{ph}N(\mathbf{q},t)=\frac{N(\mathbf{q})}{q^3}2A_{po}\times\int_{k=k_{minD}}^{k_{max}}P_D(k)dk\int_{u=0}^{\pi}f[k,\theta_{0D}(u)]du\ , \tag{24}$$

where A_{po} is given by Eq. (15) and P_D is similar to P_c defined by Eq. (16), namely,

$$P_D(k)=\frac{k}{(1+2\alpha^*\varepsilon)}[(1+\alpha^*\varepsilon)^{1/2}(1+\alpha^*\varepsilon')^{1/2}+\alpha^*(\varepsilon\varepsilon')^{1/2}\cos\beta_{0D}]^2\ , \tag{25}$$

with

$$\varepsilon'=\varepsilon+\hbar\omega_{LO}\ , \tag{26}$$

$$\cos\beta_{0D}=\frac{k+qs_{0D}}{(k^2+q^2+2kqs_{0D})^{1/2}}\ , \tag{27}$$

$$s_{0D}=\cos\zeta_{0D}=-\frac{q}{2k}+\frac{m^*\omega_{LO}}{\hbar kq}[1+\alpha^*(\varepsilon'+\varepsilon)]\ , \tag{28}$$

$$\cos[\theta_{0D}(u)]=s_{0D}\cos\alpha-(1-s_{0D}^2)^{1/2}\sin\alpha\cos u\ . \tag{29}$$

The lower-k limit k_{minD} is such that, in Eq. (28), $s_{0D}=\cos\zeta_{0D}\le1$, and is given by Eqs. (A14), in which ω_{LO} and q should be changed into $-\omega_{LO}$ and $-q$. As a consequence, one can draw additional curves k_{minD} vs q for phonon absorption, which depend on the valley through m^* and α^*, and which are restricted by additional q_{min} values, in the same way as for phonon emission. These curves have been drawn in Fig. 2 [squares (□) for the Γ valley, oblique crosses (×) for the L valley, of InP]. Again, k_{max} is chosen such that $f(k_{max})$ is negligible; typically, $k_{max}\approx1.6\times10^9\ m^{-1}$.

D. Phonon distribution

Carrying Eqs. (14) and (24) into Eq. (7) gives

$$A[N(\mathbf{q})+1]-BN(\mathbf{q})-[N(\mathbf{q})-N_L]=0\ , \tag{30}$$

where

$$A=\tau_L\frac{2A_{po}}{q^3}\int_{k=k_{minC}}^{k_{max}}P_c(k)dk\int_{u=0}^{\pi}f[k,\theta_{0C}(u)]du \tag{31}$$

and

$$B=\tau_L \frac{2A_{\rm po}}{q^3}\int_{k=k_{\min D}}^{k_{\max}} P_D(k)dk\int_{u=0}^{\pi} f[k,\theta_{0D}(u)]du \ . \tag{32}$$

The solution of Eq. (30) is

$$N(\mathbf{q})=\frac{N_L+A}{1+B-A} \ . \tag{33}$$

Obviously, the phonon distribution $N(\mathbf{q})$ is symmetric around $\mathbf{E}$, hence, $N(\mathbf{q})=N(q,\alpha)$, where $q=|\mathbf{q}|$ and $\alpha=(\mathbf{E},\mathbf{q})$. Therefore, we divide the $\{q,\alpha\}$ space into a mesh, and we compute $N(\mathbf{q})$ at points $\{q_i,\alpha_j\}$.

IV. THE ELECTRON BOLTZMANN EQUATION

The steady-state Boltzmann equations for the electrons are given by Eqs. (8) and (9). In these equations, $\hat{C}_{ii}f_i(\mathbf{k})$ is the sum of the probabilities that an electron, in any state $\mathbf{k}'$ in the valley number i, is scattered into state $\mathbf{k}$ of the valley belonging to the group of equivalent valleys. This includes intravalley scattering, as well as intervalley scattering between two equivalent valleys (namely L-L). Hence, if the Γ and L valleys are labeled 1 and 2, $\hat{C}_{11}$ represents intravalley scattering in the valley Γ, and $\hat{C}_{22}$ represents intravalley scattering in L plus intervalley scattering between equivalent L valleys.

$$\hat{C}_{ii}f_i(\mathbf{k})=\sum_{\mathbf{k}'\in \text{ valley } i} f_i(\mathbf{k}')P(\mathbf{k}',\mathbf{k}) \ . \tag{34}$$

$\hat{C}_{ij\neq i}$ is the "input intervalley scattering operator between nonequivalent valleys," $\hat{C}_{ij}f_j(\mathbf{k})$ is the sum of the probabilities that an electron, in any state $\mathbf{k}'$ in any valley $j\neq i$, is scattered into state $\mathbf{k}$ of valley i:

$$\hat{C}_{ij\neq i}f_j(\mathbf{k})=\sum_{\mathbf{k}'\notin \text{ valley } i} f_j(\mathbf{k}')P(\mathbf{k}',\mathbf{k}) \ . \tag{35}$$

Intravalley scatterings involves acoustic deformation potential (ac), piezoelectric (pi), impurity (im), intravalley nonpolar optical phonon (np) in L (not in Γ), and polar-optical-phonon (po) scattering due to LO phonons, in the valley i (the nonelasticity of acoustic scattering is not taken into account), hence,

$$\hat{C}_{11}=\hat{C}_{\Gamma\Gamma}=\hat{C}_{\rm ac}+\hat{C}_{\rm pi}+\hat{C}_{\rm im}+\hat{C}_{\rm po} \ , \tag{36a}$$

$$\hat{C}_{22}=\hat{C}_{LL}=\hat{C}_{\rm ac}+\hat{C}_{\rm pi}+\hat{C}_{\rm im}+\hat{C}_{\rm np}+\hat{C}_{\rm po}+\hat{C}_{\text{inter equiv } L\text{-}L} \ . \tag{36b}$$

The "output scattering operator" is the sum of the probabilities that an electron, in a given state $\mathbf{k}$ in valley i, is scattered into state $\mathbf{k}'$ of any valley (including the valley i); it is the inverse relaxation time $1/\tau_i(\mathbf{k})$, defined as

$$\frac{f_i(\mathbf{k})}{\tau_i(\mathbf{k})}=\sum_{\mathbf{k}'}f_i(\mathbf{k})P(\mathbf{k},\mathbf{k}')=f_i(\mathbf{k})\sum_{\mathbf{k}'}P(\mathbf{k},\mathbf{k}') \ , \tag{37}$$

and $1/\tau_i(\mathbf{k})$ is the sum of the corresponding scattering rates, namely,

$$\frac{1}{\tau_i(\mathbf{k})}=\frac{1}{\tau_{\rm ac}(\mathbf{k})}+\frac{1}{\tau_{\rm pi}(\mathbf{k})}+\frac{1}{\tau_{\rm im}(\mathbf{k})}+\frac{1}{\tau_{\rm np}(\mathbf{k})}+\frac{1}{\tau_{\rm po}(\mathbf{k})}+\sum_j\frac{1}{\tau_{ij}(\mathbf{k})} \ . \tag{38}$$

All these scattering mechanisms are kept unchanged with respect to the usual formulation, except for polar-optical-phonon scattering, where we should take into account the displacement of the phonon distribution function with respect to thermal equilibrium. This term will be studied in Sec. V.

A. Input operator $\hat{C}_{\rm po}$

The operator $\hat{C}_{\rm po}$ is the sum of two operators, one for LO-phonon emission $\hat{C}_{\rm po-}$ and one for absorption $\hat{C}_{\rm po+}$:

$$\hat{C}_{\rm po}=\hat{C}_{\rm po+}+\hat{C}_{\rm po-} \ . \tag{39}$$

Each of these operators will be labeled $\hat{C}_{{\rm po}\lambda}$, with $\lambda=1$ for emission of a phonon, and $\lambda=-1$ for absorption of a phonon. Transforming discrete sums into integrals over $\{\mathbf{k}\}$ by using the density of states, one has

$$\hat{C}_{{\rm po}\lambda}f(\mathbf{k})=\frac{1}{8\pi^3}\int_{\mathbf{k}'}f(\mathbf{k}')P_{\rm po}(\mathbf{k}',\mathbf{k})\left[N(\mathbf{q})+\frac{\lambda+1}{2}\right]\times\delta\{\varepsilon(\mathbf{k}')-[\varepsilon(\mathbf{k})+\lambda\hbar\omega_{\rm LO}]\}d^3k' \ , \tag{40}$$

with

$$\mathbf{k}'=\mathbf{k}+\lambda\mathbf{q} \ . \tag{41}$$

In polar coordinates with $\mathbf{E}$ as the polar axis, and with the notation $\varepsilon=\varepsilon(\mathbf{k})$ and $\varepsilon'=\varepsilon(\mathbf{k}')$, Eq. (40) becomes

$$\hat{C}_{{\rm po}\lambda}f(\mathbf{k})=\frac{C_{\rm po}}{8\pi^3}\int_{k'}\int_{\theta'}\int_{\varphi'}f(\mathbf{k}')\frac{G(\mathbf{k}',\mathbf{k})}{|\mathbf{k}'-\mathbf{k}|^2}\times\left[N(\mathbf{q})+\frac{\lambda+1}{2}\right]\times\delta[\varepsilon'-(\varepsilon+\lambda\hbar\omega_{\rm LO})]\times k'^2\sin\theta' dk'd\theta'd\varphi' \ . \tag{42}$$

The Dirac function determines the radius k_0' of the sphere where integrations over the angles θ' and φ' should be performed. Since $f(\mathbf{k}')$ is obviously symmetric around $\mathbf{E}$, it does not depend on φ'. Equation (42) can be written as

$$\hat{C}_{{\rm po}\lambda}f(\mathbf{k})=\frac{C_{\rm po}k_0'^2}{8\pi^3\left|\frac{d\varepsilon}{dk'}\right|_{k_0'}}\int_{\theta'=0}^{\pi}f(k_0',\theta')\sin\theta'd\theta'\int_{\varphi'=0}^{2\pi}\frac{G(k_0',k,\beta)}{q^2}\left[N(q,\alpha)+\frac{\lambda+1}{2}\right]d\varphi' \ , \tag{43}$$

with k_0' such that $\varepsilon(k_0')=\varepsilon(k)+\lambda\hbar\omega_{\mathrm{LO}}$. Inserting C_{po} into Eq. (43) and taking $|d\varepsilon/dk'|_{k_0'}$ and $G(k_0',k,\beta)$ from Eqs. (12c) and (12d), one obtains

$$\hat{C}_{\mathrm{po}\lambda}f(\mathbf{k})=\frac{A_{\mathrm{po}}}{2}\frac{k_0'}{1+2\alpha^*\varepsilon}\int_{\theta'=0}^{\pi}f(k_0',\theta')\sin\theta' d\theta'\int_{\varphi'=0}^{2\pi}F_{\mathrm{po}}\left[N(q,\alpha)+\frac{\lambda+1}{2}\right]d\varphi' , \tag{44}$$

with

$$F_{\mathrm{po}}=\left[\frac{(1+\alpha^*\varepsilon)^{1/2}(1+\alpha^*\varepsilon')^{1/2}+\alpha^*(\varepsilon\varepsilon')^{1/2}\cos\beta}{q}\right]^2 \tag{45}$$

and A_{po} given by Eq. (15).

The integration over φ' must be performed numerically by interpolating $N(\mathbf{q})$ for each value of φ'. For that purpose q and α are computed as functions of θ' and φ'. For performing the integrals in Eq. (44), we choose $\mathbf{E}=\hat{\mathbf{z}}$, and the x axis in the plane $\{\mathbf{E},\mathbf{k}\}$ (see Fig. 3); then,

$$\cos\beta=\cos\theta\cos\theta'+\sin\theta\sin\theta'\cos\varphi' \tag{46}$$

and q is determined by Eq. (41) through

$$q^2=k^2+k_0'^2-2kk_0'\cos\beta . \tag{47}$$

The scalar product of Eq. (41) with $\hat{\mathbf{z}}$ yields

$$\cos\alpha=\lambda(k_0'\cos\theta'-k\cos\theta)/q . \tag{48}$$

B. Output term $1/\tau_{\mathrm{po}}(\mathbf{k})$

The output term $1/\tau_{\mathrm{po}}(\mathbf{k})$ is also the sum of two terms, corresponding to absorption and emission:

$$\frac{f(\mathbf{k})}{\tau_{\mathrm{po}}(\mathbf{k})}=\frac{f(\mathbf{k})}{\tau_{\mathrm{po}+}(\mathbf{k})}+\frac{f(\mathbf{k})}{\tau_{\mathrm{po}-}(\mathbf{k})} , \tag{49}$$

with

$$\frac{f(\mathbf{k})}{\tau_{\mathrm{po}\lambda}(\mathbf{k})}=\frac{f(\mathbf{k})}{8\pi^3}\int_{\mathbf{k}'}P_{\mathrm{po}}(\mathbf{k},\mathbf{k}')\left[N(\mathbf{q})+\frac{1+\lambda}{2}\right]\times\delta\{\varepsilon(\mathbf{k}')-[\varepsilon(\mathbf{k})-\lambda\hbar\omega_{\mathrm{LO}}]\}d^3k' ; \tag{50}$$

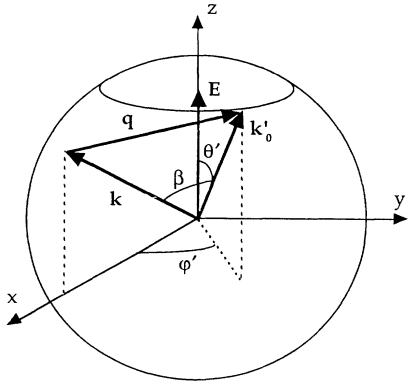

FIG. 3. Coordinate axis chosen for computing the integrals in $\hat{C}_{\mathrm{po}}$.

$\mathbf{k}'$ is given by Eq. (41). Using the same technique as that used for Eq. (40), one gets a result analogous to Eq. (44), i.e.,

$$\frac{f(\mathbf{k})}{\tau_{\mathrm{po}\lambda}(\mathbf{k})}=\frac{A_{\mathrm{po}}}{2}\frac{k_0'f(k,\theta)}{1+2\alpha^*\varepsilon}\times\int_{\theta'=0}^{\pi}\sin\theta' d\theta'\times\int_{\varphi'=0}^{2\pi}F_{\mathrm{po}}\left[N(q,\alpha)+\frac{1+\lambda}{2}\right]d\varphi' , \tag{51}$$

where A_{po} and F_{po} have the same values as they had previously, and $\mathbf{k}'=\mathbf{k}-\lambda\mathbf{q}$.

V. APPLICATION TO INDIUM PHOSPHIDE

A. Material parameters for InP

The numerical values of the material parameters used in this section are given in Appendix B. They are taken from previous studies where they had been adjusted under the assumption of LO-phonon equilibrium.

The conduction band of InP consists of one Γ valley centered at $\langle 0,0,0\rangle$, four L valleys along $\langle 1,1,1\rangle$, and three X valleys along $\langle 1,0,0\rangle$. These valleys are taken as spherical and nonparabolic, the dispersion law[14] is given by Eq. (A8). The energies of the minima of the valleys L and X are given with respect to the Γ minimum.[15–17]

As concerns the scattering mechanisms, our study included acoustic deformation-potential, piezoelectric, nonpolar optical (in the L valleys), polar-optical, and impurity scattering, which are all intravalley processes, and nonpolar optical intervalley scattering.

Acoustic deformation-potential scattering is not efficient at 300 K;[14,18] it was considered as being elastic. The transition rates and the relaxation time are taken from Refs. 19–21.

Similarly, piezoelectric scattering, having noticeable effects only at low temperature, was also treated as being elastic.[22–24]

At intermediate electric fields, below the onset of noticeable intervalley transfer, polar-optical scattering is the essential mechanism by which hot electrons relax their energy.[22,25,26] In Sec. III above we have discussed the way in which we treat this scattering mechanism in order to study nonequilibrium LO phonons.

As concerns the intervalley transfers, we took into ac-

count two types of zone-boundary phonons with their standard transition rates.[27,28] For ionized impurity scattering, we assumed equal carrier (N_c) and donor (N_D) concentrations and used the Brooks-Herring model including a screened Coulomb potential.[29–31]

For the LO-phonon relaxation we used the value $\tau_0 = 16$ ps. As explained in Sec. III A above, this choice is compatible with values determined in GaAs, which lie in the range 8–20 ps. The value 16 ps, close to the maximum 20 ps found in GaAs, takes into account the fact that the experimental thermalization times were found to depend on the surface preparation of the sample, larger values being associated with smoother surfaces.[32] Hence, the bulk values we are interested in should be nearer the highest value measured. In fact, we tried several values of τ_0 and the steady-state result did not significantly depend on τ_0. With the value 16 ps chosen, and for $T_L = 300$ K and $\hbar\omega_{LO} = 43.2$ meV, one gets $\tau_L = 5.8$ ps.

B. Simple case: Maxwellian distribution of electrons

In order to check the method, we first computed the phonon distribution function for given Maxwellian electron distributions. The calculation is then noniterative. We first set $f(\mathbf{k})$ to be the thermal-equilibrium distribution function: $f(\mathbf{k}) \propto \exp(-\varepsilon/k_B T_L)$, and found $N(q)$ equal to the equilibrium Bose-Einstein distribution N_L, checking our numerical accuracy.

We then chose a displaced Maxwellian distribution centered at $k_0 = 4\times10^7$ m^{-1} along **E**, with an electron temperature $T_e = 300$ K, which corresponds to a rough approximation of the electron distribution at $E = 2$ kV/cm. The phonon distribution was then found to depend on **q**: $N(\mathbf{q}) = N(q,\alpha)$ as shown in Fig. 4, where N is plotted versus q for three values of α. For $\alpha = 0$, corresponding to $N(q)$ in the direction of the field **E** [circles (○) on Fig. 4], $N(q,\alpha=0) \geq N_L$. In the direction opposite to the field [stars (*) on Fig. 4], $N(q,\alpha=\pi) \leq N_L$. For a direction perpendicular to the field [horizontal crosses (+) on Fig. 4], $N(q,\alpha \simeq \pi/2) \simeq N_L$. All are in agreement with earlier analytical calculations for heated and displaced Maxwellian carrier distributions.[33]

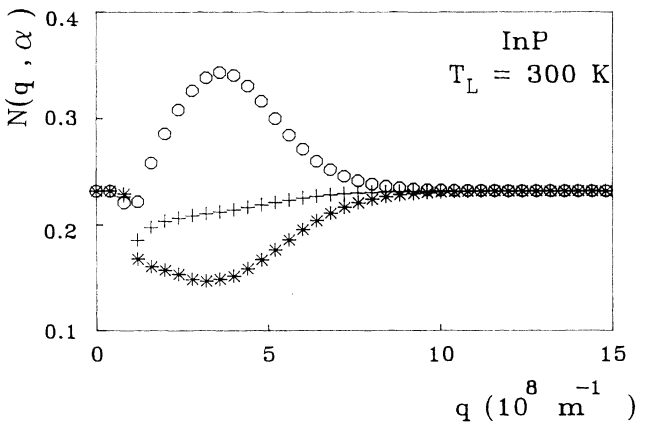

FIG. 4. Variation of $N(\mathbf{q}) = N(q,\alpha)$ vs q, for three directions α with respect to the electric field, in n-type InP, for $T_L = 300$ K and $N_D = 10^{17}$ cm^{-3}, when $f(\mathbf{k})$ is fixed to be a displaced Maxwellian centered at $k_0 = 4\times10^7$ m^{-1} and at temperature $T_e = 300$ K: $\alpha = 0$ (circles ○); $\alpha = \pi/2$ (crosses +); $\alpha = \pi$ (stars *).

C. Effects of hot electrons on the phonon distribution

In the following, we discusss the results obtained by solving Eqs. (7)–(9), by use of the iterative method described in Sec. II.

1. *Phonon distribution at a very weak electric field*

In Fig. 5(a), we have plotted (circles) $N(q,\alpha=0)$ vs q for uncompensated n-type InP, for $N_D = 10^{17}$ cm^{-3} and $T_L = 300$ K, in a very weak electric field, $E = 1$ V/cm. Even at such a weak field, the phonon distribution is disturbed from equilibrium. A peak clearly appears at low-q values

$$(0.6\times10^8 \leq q \leq 1.5\times10^8 \text{ m}^{-1}),$$

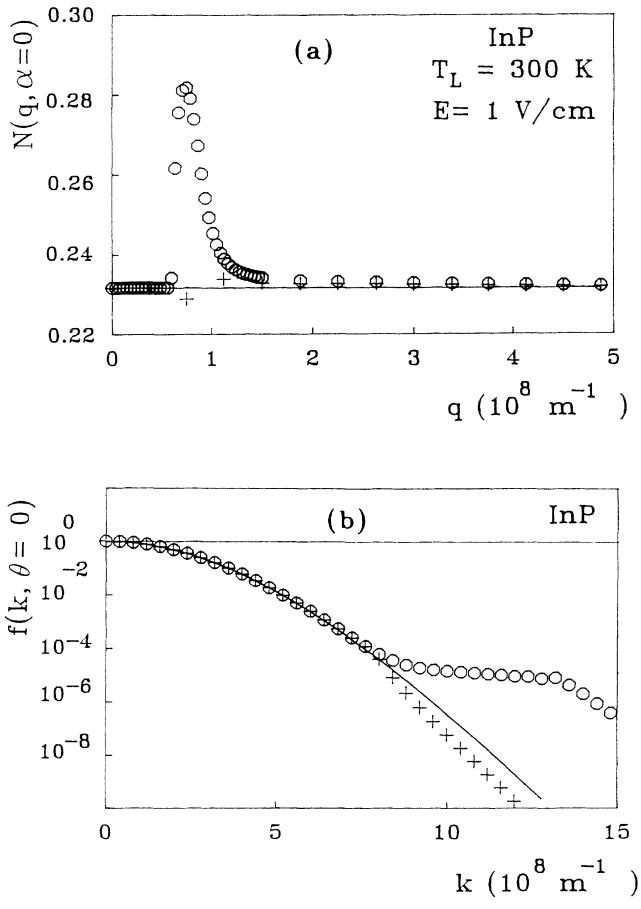

FIG. 5. Variations of $N(q,\alpha=0)$ vs q [Fig. 5(a)] and of $f(k,\theta=0)$ vs k in the Γ valley [Fig. 5(b)] for n-type InP, $T_L = 300$ K, $N_D = 10^{17}$ cm^{-3}, $E = 1$ V/cm. Circles (○): phonon distribution $N(q,\alpha=0)$ [Fig. 5(a)] and electron distribution $f(k,\theta=0)$ [Fig. 5(b)] as obtained from Eqs. (7), (8), and (9). Full line: thermal equilibrium distribution functions. Crosses (+): variations of $N(q,\alpha=0)$ [Fig. 5(a)] corresponding to an artificially modified electron distribution with $f(k,\theta=0)$ given by the crosses (+) of Fig. 5(b).

$N(q)$ being exactly equal to the thermal equilibrium Bose-Einstein distribution at higher q values. This deviation of up to 20% is quite surprising at such a low field at room temperature. Note that the horizontal scale of Fig. 5(a) has been enlarged by a factor of 10 with respect to other figures, so that only very small q values are involved in that figure.

In order to study the origin of this peak, we plotted, in Fig. 5(b), the electron distribution function for $\mathbf{k}\|\mathbf{E}$, in arbitrary units (circles). It is seen to almost coincide with the thermal-equilibrium Maxwellian distribution

$$f(\mathbf{k}) \propto \exp(-\varepsilon/k_B T_L)$$

(full line), except at large values of k, where the distribution becomes four to five orders of magnitude higher than the Maxwellian one. These numbers demonstrate the very high accuracy provided by our method even at very low values of $f(\mathbf{k})$ since, at $k=1.5\times10^9$ m^{-1}, $f(k)$ is seven orders of magnitude lower than $f(k=0)$.

It is this deviation of $f(\mathbf{k})$ from the Maxwellian, at high-k values that is responsible for the peak of $N(\mathbf{q})$ at low q values. In fact, for $N(\mathbf{q})$ being disturbed from equilibrium, one needs (i) a great number of electron–LO-phonon interactions, which always occurs at 300 K, even at thermal equilibrium, due to the wide spreading of the distribution function at this temperature and (ii) a departure of the electron distribution function from equilibrium; otherwise, due to the detailed balance of the scattering terms, $N(\mathbf{q})$ is distributed according to the Bose-Einstein relation.

In order to check this, we purposely modified the electron distribution function, at high-k values, so that $f(\mathbf{k})$ became lower than the thermal-equilibrium distribution [crosses on Fig. 5(b)]. Since this modification was made at k values where $f(\mathbf{k})$ is very small, the integral of $f(\mathbf{k})$ remained practically unchanged. The corresponding phonon distribution is plotted in Fig. 5(a) (crosses). Obviously, the peak we obtained with the actual $f(\mathbf{k})$ has now disappeared and has become a dip. This confirms that the peak at low q values in $N(\mathbf{q})$ is due to the departure of $f(\mathbf{k})$ from equilibrium at high-k values.

One could wonder that the peak is so narrow, although for a given k the q values involved extend from $q_{\min}$ to $q_{\max}$. Moreover, the higher k, the lower $q_{\min}$ and the higher $q_{\max}$, and we have just seen that the peak was due to high values of k. For example, for $k=1.3\times10^9$ m^{-1}, which corresponds to $\varepsilon=0.6$ eV, for phonon emission with $\hbar\omega_{\mathrm{LO}}=43.2$ meV, the values of q involved lie between [see Eqs. (21)]

$$q_{\min}=k(\varepsilon)-k(\varepsilon-\hbar\omega_{\mathrm{po}})=6.1\times10^7 \text{ m}^{-1}$$

and

$$q_{\max}=k(\varepsilon)+k(\varepsilon-\hbar\omega_{\mathrm{po}})=2.5\times10^9 \text{ m}^{-1} ,$$

although one can see in Fig. 5(a) that the peak extends approximately in the range

$$6\times10^7 \le q \le 1.5\times10^8 \text{ m}^{-1} .$$

This is due to the fact that, although all the values $q_{\min}\le q\le q_{\max}$ are possible, they are not all equally probable. The polar-optical-phonon transition rate $P_{\mathrm{po}}(\mathbf{k},\mathbf{k}')$ is strongly forward peaked (for example, for $k=1.3\times10^9$ m^{-1}, the probability that $\beta\le\pi/8$ [$\beta=(\mathbf{k},\mathbf{k}')$] is higher than 50%), which means that most LO scatterings involve $\mathbf{q}$ vectors close to $q_{\min}$. Finally, one should note that we are using polar coordinates, so that this disturbance involves a small number of phonons

$$N(\mathbf{q})d^3q = N(\mathbf{q})q^2\sin\alpha\, dq\, d\alpha\, du \propto q^2 ,$$

which is small, since $q\approx q_{\min}$.

Then, comparing Figs. 4, 5(a), and 5(b), one may say that, when a certain part of the electron distribution is higher (lower) than the equilibrium part, there is an increase (decrease) in the kinematically corresponding part of the phonon distribution, that is, an excess (a reduction) of phonons necessary for the establishment of the steady state.

2. *Phonon distribution at high electric field*

We have plotted $N(q,\alpha)$ and $f(k,\theta)$ in Fig. 6, again for n-type InP, $T_L=300$ K, $N_D=10^{17}$ cm^{-3}, and for an electric field $E=2$ kV/cm. $N(q,\alpha)$ is plotted versus q in Fig. 6(a), for various directions of $\mathbf{q}$ [$\alpha=0$ (circles ○), $\alpha=\pi/2$ (crosses +), $\alpha=\pi$ (stars ∗)]. $f(k,\theta)$ is plotted versus k in the Γ valley, in Fig. 6(b), for the same directions of $\mathbf{k}$ [$\theta=0$ (circles ○), $\theta=\pi/2$ (crosses +), $\theta=\pi$

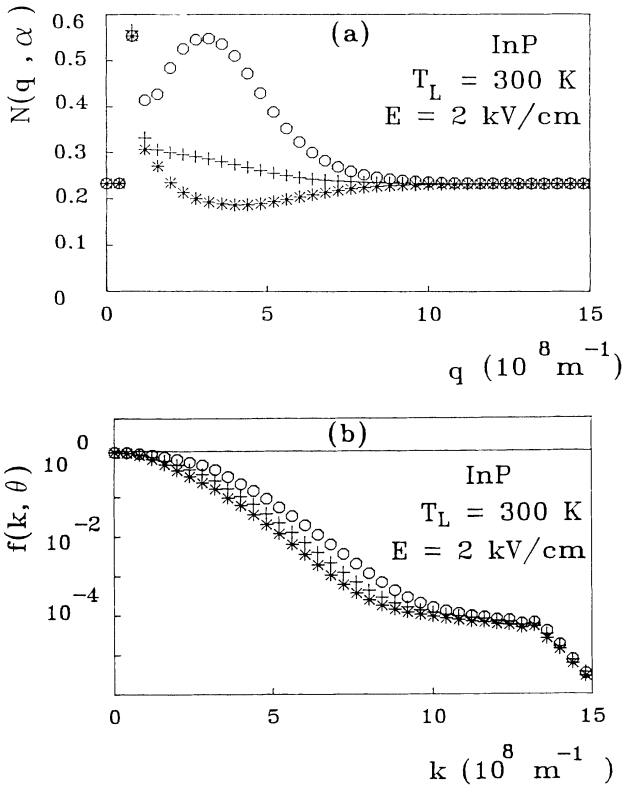

FIG. 6. Variations of $N(q,\alpha)$ vs q [Fig. 6(a)], and of $f(k,\theta)$ vs k in the Γ valley [Fig. 6(b)], for n-type InP, $T_L=300$ K, $N_D=10^{17}$ cm^{-3}, $E=2$ kV/cm. (a) Circles (○), $\alpha=0$; crosses (+), $\alpha=\pi/2$; stars ∗, $\alpha=\pi$. (b) Circles (○), $\theta=0$; crosses (+), $\theta=\pi/2$; stars (∗), $\theta=\pi$.

(stars *)]. Note that, at this electric-field strength, intervalley transfers are quite negligible, since 98% of the electrons still occupy the Γ valley.

Figure 6(a) shows that $N(q)$ has two maxima along $\alpha=0$, a single maximum in a direction transverse to the electric field $\alpha=\pi/2$, and one maximum and one minimum along $\alpha=\pi$. The position of the first peak, at low-q values of the order of 10^8 m^{-1}, does not depend on α, only its amplitude changes. Its existence was explained in Sec. V C 1 above; it is due to the increase of $f(\mathbf{k})$, at large k, with respect to the equilibrium electron distribution. This "hump" in $f(\mathbf{k})$ is well known from Monte Carlo studies of n-type GaAs.[34] It is caused by the decrease of the polar-optical scattering rates with increasing carrier energy and the correspondingly higher carrier energy in the Γ-band regions. The additional kink is due to Γ-L transfers. As shown in Fig. 6(b), the behavior of $f(k)$ at high-k values (say, $k\approx 1.3\times 10^9$ m^{-1}) is the same in all the directions θ, which explains the existence of the peak of $N(\mathbf{q})$ at low q in all directions. At intermediate k values (say, $k\approx 0.4\times 10^9$ m^{-1}), Fig. 6(b) shows that $f(k,\theta=0)$ is higher than the thermal-equilibrium distribution, which corresponds to the peak of $N(q,\alpha=0)$ [Fig. 6(a)] centered at $q\approx 0.3\times 10^9$ m^{-1}. Along $\theta=\pi/2$, $f(k,\theta=\pi/2)$ roughly coincides with $\exp(-\varepsilon/k_BT_L)$ [Fig. 6(b)], so that $N(q,\alpha=\pi/2)\approx N_L$ [Fig. 6(a)]. In the direction opposite to the electric field, $f(k,\theta=\pi)$ is lower than $\exp(-\varepsilon/k_BT_L)$ [Fig. 6(b)], which results in $N(q,\alpha=\pi)<N_L$.

Figures 7 and 8 show $N(q,\alpha)$ for the same conditions as for Fig. 6(a), but in electric fields, respectively, equal to $E=5$ kV/cm and 10 kV/cm. The amplitude of the peak in $N(q)$ at low q, in all directions, obviously increases as E increases [Figs. 6(a), 7, and 8], due to the increasing number of electrons of high energy. The second peak, centered around $q\approx 0.3\times 10^9$ m^{-1} and $\alpha=0$, is related to the fact that, even at low-k values, $f(\mathbf{k})$ departs from $\exp(-\varepsilon/k_BT_L)$. As the electric field E increases, $f(\mathbf{k})$ departs more and more from $\exp(-\varepsilon/k_BT_L)$; hence, this peak spreads in $\{\mathbf{q}\}$ space. At $E=10$ kV/cm, $f(\mathbf{k})$ strongly departs from $\exp(-\varepsilon/k_BT_L)$ at every k value, all the vectors $\mathbf{k}$ contribute to increase the number of phonons, and the two peaks of $N(q)$ merge into a single

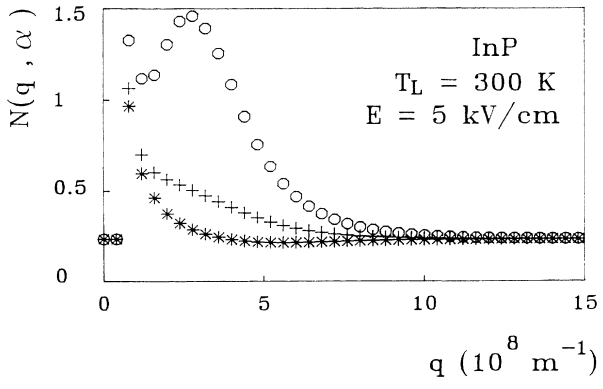

FIG. 7. Variations of $N(q,\alpha)$ vs q for n-type InP, $T_L=300$ K, $N_D=10^{17}$ cm^{-3}, $E=5$ kV/cm, along $\alpha=0$ (circles ○), $\alpha=\pi/2$ (crosses +), $\alpha=\pi$ (stars *).

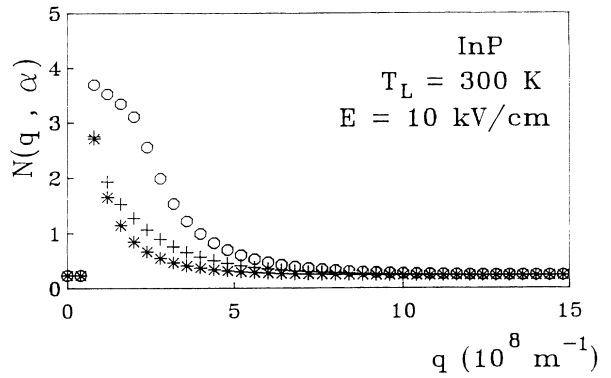

FIG. 8. Variations of $N(q,\alpha)$ vs q for n-type InP, $T_L=300$ K, $N_D=10^{17}$ cm^{-3}, $E=10$ kV/cm, along $\alpha=0$ (circles ○), $\alpha=\pi/2$ (crosses +), $\alpha=\pi$ (stars *).

one (Fig. 8). A comparison of Figs. 6(a), 7, and 8 shows that, as the electric-field strength increases, the number of phonons increases and the phonons are more and more scattered among all the directions α.

In Fig. 9, we have plotted $N(q,\alpha=0)$ vs q, at different electric-field strengths, in the range 1–50 kV/cm. Up to 10 kV/cm, Fig. 9(a) illustrates the above explanations: the intensity of the peak centered at $q\approx 0.3\times 10^9$ m^{-1} increases and the peak broadens. At higher electric fields

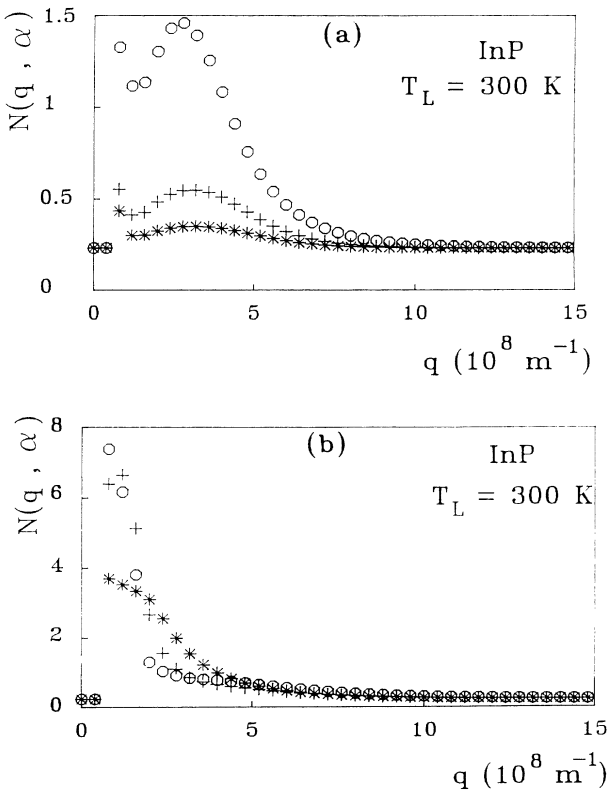

FIG. 9. Comparison of the variations of $N(q,\alpha=0)$ vs q along the electric field for n-type InP, $T_L=300$ K, $N_D=10^{17}$ cm^{-3}, at different electric-field strengths: (a) $E=1$ kV/cm (stars *); 2 kV/cm (crosses +); 5 kV/cm (circles ○). (b) $E=10$ kV/cm (stars *); 20 kV/cm (crosses +); 50 kV/cm (circles ○).

[see Fig. 9(b)], intervalley transfers from Γ to L increase significantly, the maximum value of $f(\mathbf{k})$ shifts towards higher values of k (see below), hence, the peak in $N(q,\alpha=0)$ shifts towards lower values of q due to the anisotropy of the LO-phonon scattering, which enhances scattering processes at $q_{\min}$ as explained in Sec. V C 1 above.

Finally, the influence of the carrier concentration is shown in Fig. 10, where $N(q,\alpha=0)$ is plotted versus q, in InP, at 300 K, $E=5$ kV/cm, for two-carrier (equal to donor) concentrations $N_D=1\times10^{17}$ cm^{-3} [circles ($\circ$) in Fig. 10] and $N_D=2\times10^{17}$ cm^{-3} [stars ($*$) in Fig. 10]. Figure 10 demonstrates that the phonon distribution strongly depends on N_D, since the number of nonthermal phonons increases with increasing N_D.

D. Effect of hot phonons on the electron distribution

In the preceding section we showed that hot electrons introduce important disturbances of the phonon distribution. The purpose of this section is to study the influence of the phonon disturbances on the electron distribution or, more precisely, to study the differences between the hot-electron distribution computed assuming, as usual, that the phonons are in thermal equilibrium, and the electron distribution computed taking into account nonequilibrium phonons.

We remember that our iterative process is such that, at the first iteration, the electron distribution function is computed for phonon equilibrium. Therefore, we should study the difference between the electron distributions obtained at the first and last iterations.

1. Electron distribution function in the Γ valley

In Figs. 11(a)–11(f), we have plotted, for various electric-field strengths in the range 1–50 kV/cm, the electron distribution function along the electric field, that is, $f(k_z)=f(k_x=0,k_y=0,k_z)=f(k,\ \theta=0$ and $\theta=\pi)$, vs k_z in the Γ valley. A comparison is made between $f(k_z)$ computed, as usual, assuming the phonons to be at thermal equilibrium (crosses), and $f(k_z)$ computed taking into account hot LO phonons (circles), in n-type InP,

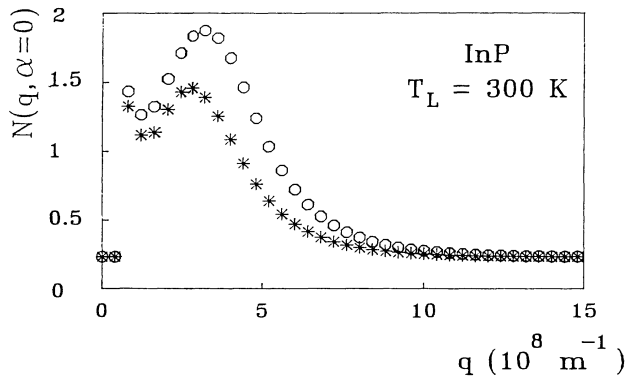

FIG. 10. Comparison of the variations of $N(q,\alpha=0)$ vs q along the electric field for n-type InP, $T_L=300$ K, $E=5$ kV/cm, at different impurity (equal to carrier) concentrations: $N_D=1\times10^{17}$ cm^{-3} (stars $*$) and $N_D=2\times10^{17}$ cm^{-3} (circles $\circ$).

for $T_L=300$ K and $N_D=1\times10^{17}$ cm^{-3}. The kink in $f(\mathbf{k})$, which appears at $k=1.3\times10^9$ m^{-1} in Fig. 6(b), is also present in Figs. 11(a)–11(f), but cannot be seen in Figs. 11(a)–11(d), which are drawn using a linear scale on the ordinate axis. This kink is always due to intervalley transfers, and its position is thus independent of $N(\mathbf{q})$.

At $E=1$ kV/cm [Fig. 11(a)], the electron distribution is not significantly disturbed by hot phonons, due to the fact that the phonon disturbance is small [Fig. 9(a)]. A significant deviation begins to appear at $E=2$ kV/cm [Fig. 11(b)], with a decrease of $f(k)$ at low k and an increase at high k.

This effect increases and becomes quite important at $E=5$ kV/cm [Fig. 11(c)]. The effect of hot phonons is qualitatively the same as the effect of increasing the electric field.[35] This can be explained in the following way. At intermediate fields, where the energy relaxation of electrons involves mainly LO phonons, electrons transfer energy to the phonons, the average energy of which increases (the "phonon temperature" becomes higher than the lattice temperature). As a consequence, the electrons relax less energy than if the phonons were at equilibrium since, roughly speaking, the electron-energy relaxation is proportional to the difference between the electron and the phonon temperatures. So the average electron energy is higher than if the phonons were at thermal equilibrium. Hence, the effect of hot phonons on the electrons is qualitatively the same as the effect of increasing the electric field while maintaining the phonons at thermal equilibrium.

The disturbance of the electron distribution due to hot phonons is largest (50% at the maximum) at $E=10$ kV/cm [Fig. 11(d)], which is the characteristic field in InP where the steady-state velocity reaches its peak value. At this electric field, intervalley transfers between the Γ valley and the L valleys become important. Figure 11(e) shows that at $E=20$ kV/cm, the electron distribution function spreads widely in $\{\mathbf{k}\}$ space and is strongly distorted, but the discrepancy between the two distributions is only 30% at the maximum of $f(\mathbf{k})$.

At $E=50$ kV/cm [Fig. 11(f)], the predominant mechanism of electron energy relaxation is, by far, intervalley scattering. LO phonons play no significant role, and their disturbance has practically no effect on the electron distribution, as can be seen in Fig. 11(f).

2. Electron distribution function in the L valleys

In Figs. 12(a)–12(c) we have plotted, for various electric-field strengths, the electron distribution function along the electric field, that is, $f(k_z)=f(k_x=0,k_y=0,k_z)=f(k,\ \theta=0$ and $\theta=\pi)$, vs k_z in the L valleys. A comparison is made between $f(k_z)$ computed as usual assuming the phonons in thermal equilibrium (crosses), and $f(k_z)$ computed taking into account hot LO phonons (circles), in n-type InP, for $T_L=300$ K and $N_D=1\times10^{17}$ cm^{-3}.

At $E=2$ kV/cm [Fig. 12(a)], the distribution function in the L valleys has a very regular shape. The effect of hot phonons, as in the Γ valley, is to lower and broaden the peak of the distribution function. We once more

stress the great accuracy obtained with our method, which had already been pointed out with regard to the phonon distribution function, but is also remarkable for the electron distribution: the maximum value of $f(\mathbf{k})$ in the L valleys, as shown in Fig. 12(a), is 3.5×10^{-28}, as compared to 1.5×10^{-26} in the Γ valley [see Fig. 11(b)]. So the distribution function shown in Fig. 12(a) concerns only 2% of the electrons since, at $E=2$ kV/cm, 98% of the electrons still populate the Γ valley.

In the L valleys as well as in the Γ valley, the maximum effect of hot phonons occurs at $E=10$ kV/cm [see Fig. 12(b)]. It is remarkable that the relative changes of $[f(\mathbf{k})]_{max}$ for the two-electron distribution functions are about the same in the Γ and L valleys for all fields [compare Figs. 11(b), 11(d), and 11(e) to Figs. 12(a), 12(b), and 12(c)]. Above the threshold field of 10 kV/cm the effect of

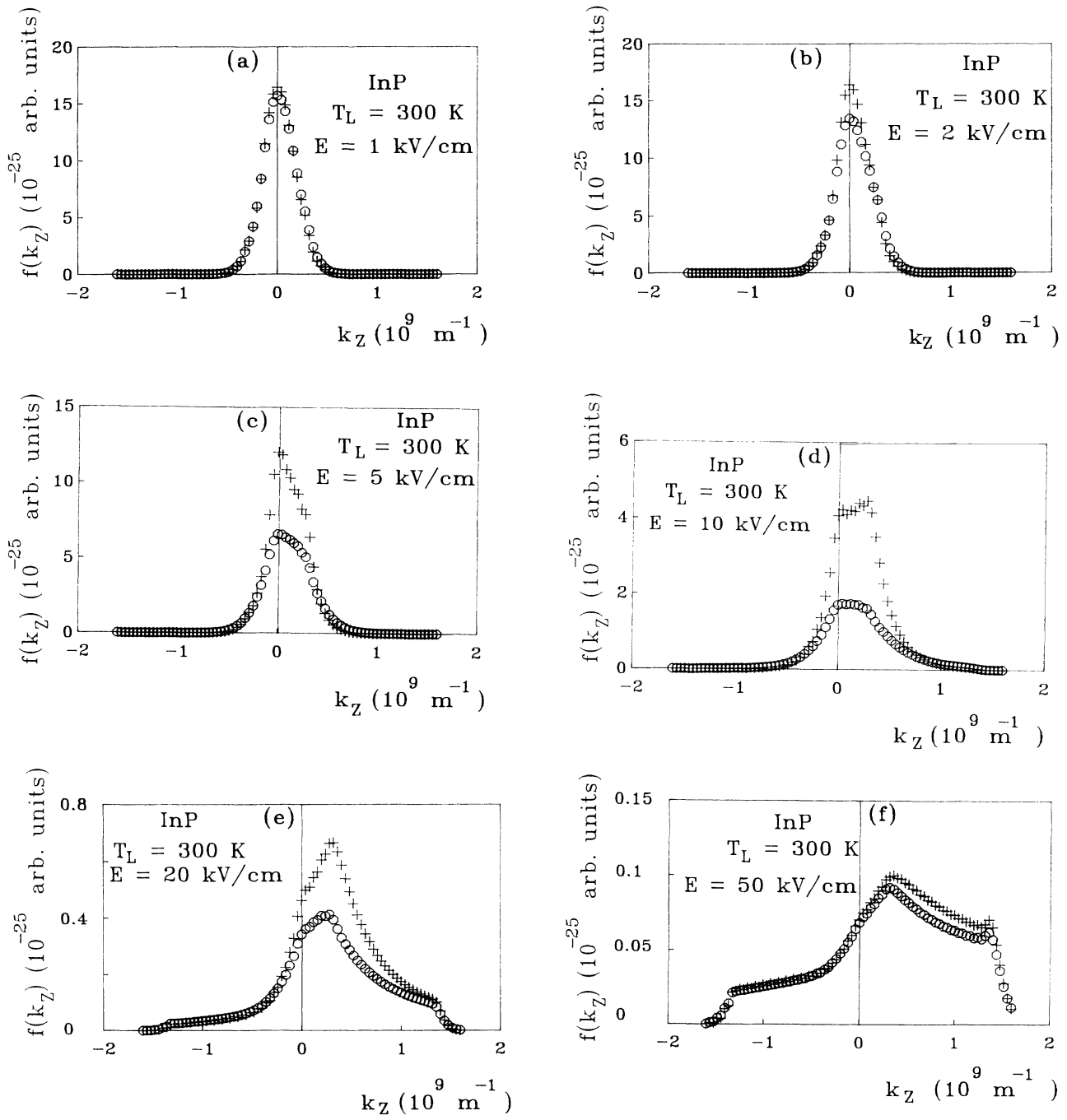

FIG. 11. Electron distribution function $f(k_z)=f(k_x=0,\ k_y=0,k_z)$ along the electric field vs k_z, in the Γ valley of InP, for $T_L=300$ K and $N_D=1\times10^{17}$ cm^{-3}. Comparison between $f(k_z)$ computed assuming phonon equilibrium (crosses +) and $f(k_z)$ computed taking into account hot LO phonons (circles ○) at various electric-field strengths. (a) $E=1$ kV/cm; (b) $E=2$ kV/cm; (c) $E=5$ kV/cm; (d) $E=10$ kV/cm; (e) $E=20$ kV/cm; (f) $E=50$ kV/cm.

hot phonons on the carrier distribution decreases in both types of valleys [see Figs. 11(f) and 12(c)]: LO phonons become less efficient as compared to intervalley phonons.

E. Effect of hot phonons on electronic transport parameters

In Sec. V D we have detailed how the electron distribution function is modified by hot phonons. As a consequence, all electronic-transport parameters, being average values over the carrier distribution, are also modified. The purpose of Sec. V E is to study the magnitude of these modifications. Therefore, as was done in Secs. V A–V D, we shall compare transport parameters computed assuming phonon equilibrium with those computed taking into account LO-phonon heating. Again, all calculations were performed for n-type InP, $T_L=300$ K, $N_D=1\times10^{17}$ cm^{-3}, and for $E\leq 50$ kV/cm. In the tables of Appendix C, we summarize our numerical results, which are also graphically displayed in Figs. 13–15.

The average electron energy is plotted versus E in Fig. 13. The full lines are the results obtained for phonons assumed to be at equilibrium and the circles represent results obtained by taking into account hot phonons. The effect of hot phonons is clearly to increase the average energy of the electrons, as explained above. It is difficult to investigate in detail the increase in electron energy due to hot phonons, since this increase depends on the origin taken: for example, in the L valley, the increase of 8 meV (from 658 to 666 meV) at 1 kV/cm (see Appendix C) represents only 1.2% with reference to the bottom of the Γ valley, but represent 80% with reference to the thermal energy of 648 meV of the electrons in the L valley. The energy increase due to hot phonons reaches 50% of the electron average energy at 10 kV/cm.

One might think that the increase in the electron energy, in particular, in the Γ valley, due to hot phonons, would result in an increase of Γ-L intervalley transfers, and thus would enhance the population of L valleys. This is, in fact, not so simple, as shown in Fig. 14 where the populations of the valleys are plotted versus the electric field: in that figure, too, the full lines are the values obtained assuming the phonons to be at thermal equilibrium, and the circles are the values computed taking into account hot phonons. This figure, using the numerical values of Appendix C, shows that at low electric field, hot phonons keep electrons in the Γ valley, and that only above 7 kV/cm hot phonons increase Γ-to-L transfers and enhance the population of L valleys. This is due to the fact that the populations of the valleys are a result of a balance between Γ-to-L and L-to-Γ transfers.

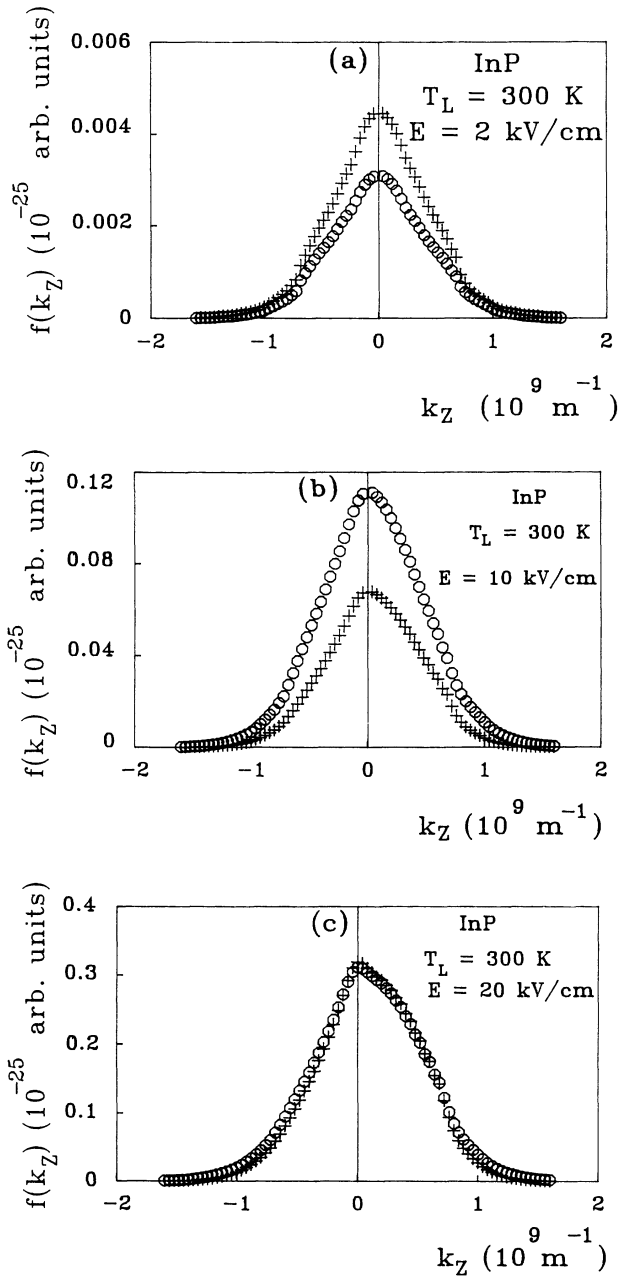

FIG. 12. Electron distribution function $f(k_z)=f(k_x=0, k_y=0, k_z)$ along the electric field vs k_z in the L valleys of InP for $T_L=300$ K and $N_D=1\times10^{17}$ cm^{-3}. Comparison between $f(k_z)$ computed assuming phonon equilibrium (crosses) and $f(k_z)$ computed taking into account hot LO phonons (circles) at various electric-field strengths. (a) $E=2$ kV/cm; (b) $E=10$ kV/cm; (c) $E=20$ kV/cm.

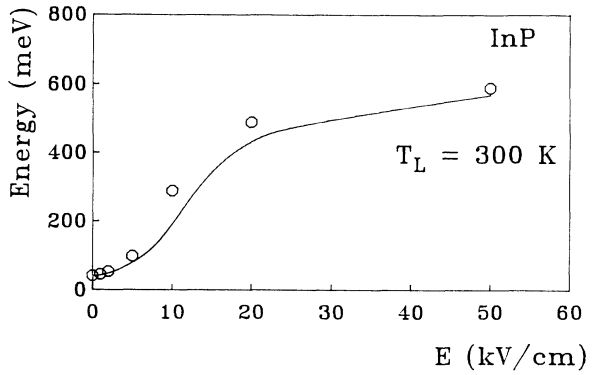

FIG. 13. Variations vs the electric field of the average electron energy in InP for $T_L=300$ K and $N_D=1\times10^{17}$ cm^{-3}, computed assuming the phonons to be at thermal equilibrium (full line), and taking into account hot LO phonons (circles).

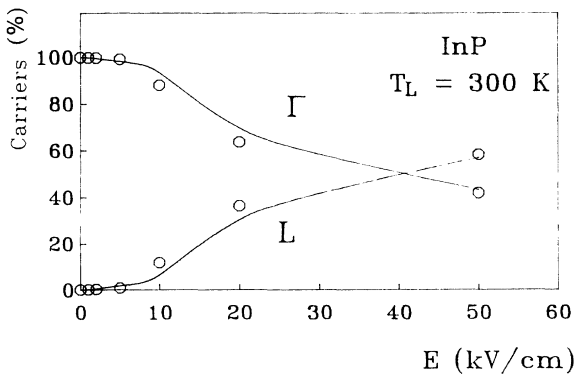

FIG. 14. Variations vs the electric field of the proportions of electrons in the Γ and L valleys in InP for $T=300$ K and $N_D=1\times10^{17}$ cm^{-3}, computed assuming the phonons to be at thermal equilibrium (full line), and taking into account hot LO phonons (circles).

At low field, 2 kV/cm, for example, the effect of hot phonons in both valleys [see Figs. 11(b) and 12(a)] is to decrease the number of carriers of low k and to increase the number of carriers of high k, hence in the Γ valley to enhance Γ-to-L transfers, and in the L valley to enhance L-to-Γ transfers. It turns out that at this field the latter prevails over the former, due to the fact that Γ-to-L transfers are produced only by the very few electrons in Γ with an energy higher than $\approx$610 meV, a number that increases very little due to hot phonons at low fields. Conversely, a small increase of the number of carriers in L valleys at every k, and even at low k, enhances L-to-Γ transfers. As a consequence, at low fields, the increase of the number of carriers due to hot phonons in the Γ valley, occurring mostly at energies lower than 610 meV, produces very few additional Γ-to-L transfers, although the increase of the number of carriers at low k in the L valleys, due to hot phonons, increases significantly the L-to-Γ transfers; hence, additional L-to-Γ transfers dominate additional Γ-to-L transfers due to hot phonons at low fields, thus increasing the number of carriers in the Γ valley. Nevertheless, a decrease in the population [i.e., of the integral of $f(\mathbf{k})$] in the L valleys remains consistent with an increase of the average energy [i.e., of the integral of $\varepsilon f(\mathbf{k})$] in this valley, due to the weighting factor ε roughly proportional to k^2.

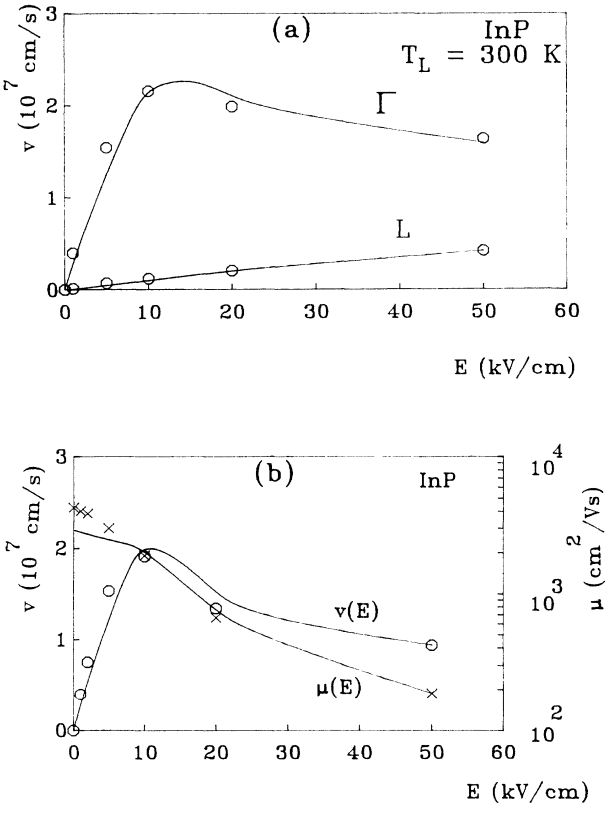

FIG. 15. Variations vs the electric field in InP for $T_L=300$ K and $N_D=1\times10^{17}$ cm^{-3} of the average electron velocities, computed assuming phonons to be at thermal equilibrium (full line) and taking into account hot LO phonons (circles and crosses). (a) Mean velocities in the Γ and L valleys. (b) Drift velocity and mobility.

At higher field ($E\geq7$ kV/cm in InP), electrons in the Γ valley are strongly heated by the field, their k values spread around the energy of 610 meV, allowing Γ-to-L transfers; hence, hot phonons increase the number of electrons at energies above this value. Thus, the effect of hot phonons is to enhance Γ-to-L transfers more than L-to-Γ transfers, this being reinforced since there are more electrons in Γ than in L. At 10 kV/cm, 10% of the carriers populate the L valleys taking into account hot phonons, although only 6% populate the L valleys if one assumes the phonons to be at thermal equilibrium (see Appendix C). At very high fields, as explained above, LO-phonon scattering becomes negligible with respect to intervalley transfers, thus hot phonons have no effect on the valley populations.

The mean steady-state carrier velocity (drift velocity) is the most important transport parameter, since it can be measured experimentally.[36–38] Our theoretical results are plotted versus the electric-field strength E in Fig. 15. Figure 15(a) shows the average Γ- and L-valley velocities, and Fig. 15(b) the overall mean velocity (drift velocity). Full lines are results obtained with phonons at thermal equilibrium, while circles take into account hot phonons. Hot-phonon effects cause significant changes in the drift velocity at fields below 10 kV/cm: the variation induced by hot phonons reaches 44% at 1 kV/cm, 42% at 2 kV/cm, and 28% at 5 kV/cm.

The Ohmic mobility, which was found to be 3075 cm^2/Vs with phonons at thermal equilibrium, reaches 4200 cm^2/Vs taking into account the phonon disturbance (see Appendix C). Here it is the displacement of the phonon distribution in $\mathbf{q}$ space that leads to reduced frictional effect of the LO phonons on the carrier drift. These results (phonon-drag effect) confirm the very similar theoretical predictions for n-type GaAs within the carrier-temperature[8] and Monte Carlo approaches.[7] It should be noted that, at such low fields as those investigated for the Ohmic mobility study ($E=10$ V/cm), one should make sure that the mesh in $\{\mathbf{k}\}$ space is small

enough; otherwise, important errors may occur. For example, with 20 steps along k, the Ohmic mobility is found to be 2870 cm^2/Vs; it reaches the value of 4200 cm^2/Vs only when the number of steps becomes larger than 40.

VI. CONCLUSION

In the present paper we extended the matrix method, which had previously been used for theoretically determining the non-Ohmic steady state for phonon equilibrium, to the solution of the three coupled Boltzmann equations for the Γ- and the L- valley electrons and the LO phonons. We devised an iterative process, enabling us to construct first the electron distribution function with phonons at thermal equilibrium, which is the usual way of investigating hot-carrier behavior, and from there to converge towards the steady-state distribution functions of both hot electrons and nonequilibrium LO phonons.

In this way, the departure of the phonon distribution $N(\mathbf{q})$ from thermal equilibrium was studied in detail. The main features are the following.

(i) $N(\mathbf{q})$ departs from the thermal-equilibrium distribution N_L due to the departure of the electron distribution function $f(\mathbf{k})$ from $\exp(-\varepsilon/k_B T_L)$.

(ii) At weak fields, along the directions where $f(\mathbf{k}) > \exp(-\varepsilon/k_B T_L)$, $N(\mathbf{q})$ is larger than N_L, and along the directions where $f(\mathbf{k}) < \exp(-\varepsilon/k_B T_L)$, $N(\mathbf{q})$ is smaller than N_L.

(iii) A departure of $f(\mathbf{k})$ from equilibrium at a higher k value results in a departure of $N(\mathbf{q})$ from equilibrium at a lower q value.

(iv) At all fields, even very weak ones, a narrow peak in the phonon distribution develops at low q values ($q \approx 0.6\times 10^8$ m^{-1}). It is caused by the distortion, at high k values, of the electron distribution due to the combined action of carrier heating, by the field, of LO-phonon scattering and of intervalley transfers; this latter effect, producing a kink in the electron distribution function at $k = 1.3\times 10^9$ m^{-1} corresponding to the Γ-L energy separation (610 meV), is mainly responsible for that narrow peak in the phonon distribution. At intermediate fields (below the threshold field $E \approx 10$ kV/cm), the phonon distribution exhibits a second and wide peak due to the overall heating of the electron distribution. As the electric field increases, this latter peak broadens, then merges with the former one, and at high field ($E > 10$ kV/cm) shifts towards lower q values. At the same time, the departure of $N(\mathbf{q})$ from N_L increases.

We showed that, in turn, the electron distribution function is strongly affected by nonequilibrium LO phonons. The effect of the phonon disturbances is to enhance hot-carrier effects, at fields lower than 10 kV/cm, by lowering the momentum and energy relaxation of the electrons as consequence of the increasing phonon amplification. The perturbation of the electron distribution is highest at 10 kV/cm and reaches 50% at the maximum value of $f(\mathbf{k})$. At high fields (≥ 20 kV/cm), hot phonons do not significantly affect the electron distribution function, since intervalley scattering is by far the dominant carrier relaxation process.

As a consequence of the nonequilibrium-phonon-induced perturbation of the electron distribution, electron transport parameters are significantly modified. At low fields, hot phonons enhance more L-to-Γ than Γ-to-L transfers; hence, the proportion of electrons in the L valleys is lowered due to hot phonons, but at higher field ($E \geq 7$ kV/cm) this effect is reversed; hence, hot phonons increase the proportion of carriers in the L valleys. At every field the average energy of the carriers is increased, e.g., by 47% at 10 kV/cm.

The carrier drift velocity is also significantly modified. The peak velocity is shifted towards lower electric fields, and in the range 0–10 kV/cm the velocity is increased by hot-phonon effects, up to an amount of 45%. The Ohmic mobility is also strongly modified, changing its value from 3075 cm^2/Vs for phonon equilibrium, to 4200 cm^2/Vs when nonequilibrium LO phonons are taken into account, representing an increase of 37%.

Two important consequences arise from the present work.

(i) We have presented a method which allows one to calculate coupled steady-state hot-phonon and hot-electron distribution functions with an accuracy far beyond other existing methods.

(ii) Taking into account LO-phonon disturbances significantly modifies electron distribution functions and electron transport parameters, in particular the carrier drift velocity. As a consequence, a new set of carrier-phonon coupling constants should be derived by fitting the curves to experimental results.

ACKNOWLEDGMENTS

Centre d'Electronique de Montpellier is Laboratoire associé au Centre National de la Recherche Scientifique (URA No. 391). This work was supported by the European Networks of the French "Ministère de la Recherche et de l'Enseignement Supérieur" and the French "Ministère des Affaires Etrangères", by the French C3NI (Centre de Compétences en Calcul Numérique Intensif), and by Contract No. ESPRIT BRA 3017.

APPENDIX A: PHONON EMISSION OPERATOR $\hat{C}_{ph}$

We use polar coordinates with polar axes along $\mathbf{q}$ (see Fig. 1) so that $\mathbf{k} = \{k, \zeta, u\}$ and

$$f(\mathbf{k}) = f(k,\zeta,u) ,$$

$$\varepsilon(\mathbf{k}-\mathbf{q}) - [\varepsilon(\mathbf{k}) - \hbar\omega_{LO}] = H_c(k,q,\zeta) , \tag{A1}$$

$$G(\mathbf{k}-\mathbf{q},\mathbf{k}) = G(k,q,\zeta) .$$

Equation (12a) is then written as

$$\hat{C}_{ph} N(\mathbf{q}) = \frac{[N(\mathbf{q})+1]}{q^2} 2C_{po} I_c , \tag{A2}$$

where

$$I_c=\int_{k=0}^{\infty}k^2dk\int_{u=0}^{2\pi}du\int_{\zeta=0}^{\pi}G(k,q,\zeta)f(k,u,\zeta)\times\delta[H_c(k,q,\zeta)]\sin\zeta\,d\zeta\ . \tag{A3}$$

With $\cos\zeta=s$, Eq. (A3) can be written as

$$I_c=\int_{k=0}^{\infty}k^2dk\int_{u=0}^{2\pi}J_c\,du\ , \tag{A4}$$

with

$$J_c=\int_{s=-1}^{+1}G(k,q,s)f(k,u,s)\delta[H_c(k,q,s)]ds\ . \tag{A5}$$

Since H_c is an increasing function of s, Eq. (A5) can be written as

$$J_c=\int\frac{G(k,q,s)f(k,u,s)\delta[H_c(k,q,s)]}{|\partial H_c/\partial s|}dH_c\ ; \tag{A6}$$

thus,

$$I_c=\int_{u=0}^{2\pi}\int_{k=0}^{\infty}\frac{G(k,q,s_0)f(k,u,s_0)}{|\partial H_c/\partial s|_{s=s_0}}k^2dk\,du\ , \tag{A7}$$

with s_0 such that $H_c(k,q,s_0)=0$. We shall now determine the various quantities involved in Eq. (A7).

Determination of s_0. By using the dispersion relation

$$\varepsilon(\mathbf{k})[1+\alpha^*\varepsilon(\mathbf{k})]=\frac{\hbar^2k^2}{2m^*} \tag{A8}$$

one gets, solving the second-order equation (A8),

$$\varepsilon(\mathbf{k})=\frac{1}{2\alpha^*}\left[-1+\left[1+4\alpha^*\frac{\hbar^2k^2}{2m^*}\right]^{1/2}\right]\ . \tag{A9}$$

Carrying Eq. (A9) into (A1) gives $s_0=\cos\zeta_0$ as a solution of

$$\frac{1}{2\alpha^*}\left\{-1+\left[1+4\alpha^*\frac{\hbar^2(\mathbf{k}-\mathbf{q})^2}{2m^*}\right]^{1/2}\right\}=\frac{1}{2\alpha^*}\left\{-1+\left[1+4\alpha^*\frac{\hbar^2k^2}{2m^*}\right]^{1/2}\right\}-\hbar\omega_{\mathrm{LO}} \tag{A10}$$

with

$$(\mathbf{k}-\mathbf{q})^2=k^2+q^2-2kq\cos\zeta_0=k^2+q^2-2kqs_0\ . \tag{A11}$$

Equation (A10) can then be easily solved, giving

$$s_0=\frac{q}{2k}-\frac{m^*\alpha^*\omega_{\mathrm{LO}}^2}{kq}+\frac{m^*\omega_{\mathrm{LO}}}{\hbar kq}\left[1+4\alpha^*\frac{\hbar^2k^2}{2m^*}\right]^{1/2}\ . \tag{A12}$$

One can show that

$$s_0=\frac{q}{2k}+\frac{m^*\omega_{\mathrm{LO}}}{\hbar kq}[1+\alpha^*(\varepsilon'+\varepsilon)] \tag{A13}$$

with

$$\varepsilon'=\varepsilon(\mathbf{k}-\mathbf{q})=\varepsilon-\hbar\omega_{\mathrm{LO}}\ ,$$

thus $s_0>0$.

Limitation of the integration domain over k. Since $s_0=\cos\zeta_0$, one should have $s_0\le1$, which, carried into Eq. (A12), yields

$$k\ge k_{\mathrm{min}C}\ , \tag{A14a}$$

$$k_{\mathrm{min}C}=[-B+\sqrt{B^2-4AC}\,]/(2A)\ , \tag{A14b}$$

$$A=\frac{\hbar^2q^2}{m^{*2}\omega_{\mathrm{LO}}^2}-\frac{4\alpha^*\hbar^2}{2m^*}\ , \tag{A14c}$$

$$B=\frac{2\hbar q}{m^*\omega_{\mathrm{LO}}}\left[-\frac{\hbar q^2}{2m^*\omega_{\mathrm{LO}}}+\alpha^*\hbar\omega_{\mathrm{LO}}\right]\ , \tag{A14d}$$

$$C=\left[-\frac{\hbar q^2}{2m^*\omega_{\mathrm{LO}}}+\alpha^*\hbar\omega_{\mathrm{LO}}\right]^2-1\ . \tag{A14e}$$

These equations show that $k_{\mathrm{min}C}$ is a function of q, which depends on the valley through m^* and α^*. It is then possible to plot $k_{\mathrm{min}C}$ vs q in valley Γ and valley L, which was done in Fig. 2 [circles ($\circ$) and horizontal crosses (+)] for InP.

Equation (A14b) requires that $B^2-4AC\ge0$, which gives a condition on q, obtained from Eqs. (A14c)–(A14e). The calculation is tedious but straightforward and yields

$$q\ge q_{\mathrm{min}}=\omega_{\mathrm{LO}}\sqrt{2\alpha^*m^*}\ . \tag{A15}$$

This relation can be demonstrated geometrically as follows: for a given $\mathbf{k}$ vector, the value $\Delta k=q=|\mathbf{q}|$ is minimum when the vector $\mathbf{k}'=\mathbf{k}-\mathbf{q}$, after the collision, is parallel to $\mathbf{k}$. Then, a minimum value of q corresponds to each $\mathbf{k}$ vector. The absolute minimum is reached when the variation Δk corresponding to the energy loss is minimum, which is obtained at high energy. Then,

$$\varepsilon(1+\alpha^*\varepsilon)\approx\alpha^*\varepsilon^2=\frac{\hbar^2}{2m^*}k^2\ ,\qquad \varepsilon=\frac{\hbar k}{(2\alpha^*m^*)^{1/2}}\ . \tag{A16}$$

When ε varies by the amount $\Delta\varepsilon=\hbar\omega_{\mathrm{po}}$, then k varies by the amount $\Delta k=q_{\mathrm{min}}$, and Eq. (A16) gives

$$\hbar\omega_{\mathrm{LO}}=\frac{\hbar q_{\mathrm{min}}}{(2\alpha^*m^*)^{1/2}}\ , \tag{A17}$$

which is Eq. (A15). In practice, of course, one is not able to investigate k up to infinity; k has to be limited to an upper value k_{max} chosen such that $f(k_{\mathrm{max}})$ is negligible. In practice, one may limit oneself to $k_{\mathrm{max}}=1.6\times10^9$ m^{-1}. The corresponding value $\varepsilon_{\mathrm{max}}=\varepsilon(k_{\mathrm{max}})$ determines the values q_{min} and q_{max} as given in Eq. (21) of Sec. III A.

Finally, one should note that k should be such that $k\ge k_{\mathrm{min}C}$, and also such that $\varepsilon\ge\hbar\omega_{\mathrm{LO}}$. In fact, one can show that the latter is automatically satisfied provided $k\ge k_{\mathrm{min}C}$.

Determination of $|\partial H_c/\partial s|_{s=s_0}$. From Eq. (A1), with $s=\cos\zeta$ and $\zeta=(\mathbf{q},\mathbf{k})$, we get

$$\frac{\partial H_c}{\partial s}=\frac{\partial\varepsilon(\mathbf{k}-\mathbf{q})}{\partial s}\ , \tag{A18a}$$

and from Eq. (A9)

$$\varepsilon(\mathbf{k}-\mathbf{q})=\frac{1}{2\alpha^*}\left\{-1+\left[1+\frac{4\alpha^*\hbar^2}{2m^*}\times(k^2+q^2-2kqs)\right]^{1/2}\right\}. \tag{A18b}$$

With Eqs. (A18a) and (A9) this gives

$$\left|\frac{\partial H_c}{\partial s}\right|=\frac{\hbar^2 kq}{m^*}\frac{1}{1+2\alpha^*\varepsilon(\mathbf{k}-\mathbf{q})}. \tag{A19}$$

Determination of $G(k,q,s_0)$. From Eq. (12c), the determination of $G(k,q,s_0)$ is that of $\cos\beta_0$ with $\xi=(\mathbf{q},\mathbf{k})$ and $\beta=(\mathbf{k},\mathbf{k}-\mathbf{q})$ (see Fig. 1). Simple algebra gives, with $s_0=\cos\xi_0$,

$$\cos\beta_0=\frac{k-qs_0}{(k^2+q^2-2kqs_0)^{1/2}}. \tag{A20}$$

Determination of $f(k,u,s_0)$. The electron distribution $f(\mathbf{k})$ is determined in polar coordinates with polar axes along the electric field **E**, since it is symmetric around **E**. Then $f(\mathbf{k})=f(k,\theta)$ has to be expressed in the axis related to **q**. More precisely (see Fig. 1), one defines two sets of axes: the axes $(T)=\{x,y,z\}$ with axis z along **E**, and $(T')=\{x',y',z'\}$ with axis z' along **q**. Since we have great freedom in our choice of axes $\{x,y,x',y'\}$, we choose $y=y'$ perpendicular to the plane $\{z,z'\}$ (see Fig. 1). This determines the axes x and x' (x and x' lie in the plane $\{z,z'\}$). We label **x**, **y**, **z**, **x'**, **y'**, **z'**, the unit vectors of the axes x, y, z, x', y', z'. If the subscripts (T) and (T') refer to coordinates with respect to axes (T) and (T'), one has

$$\mathbf{k}_{(T)}=\begin{bmatrix}k\\ \theta\\ \varphi\end{bmatrix}\quad \mathbf{k}_{(T')}=\begin{bmatrix}k\\ \xi\\ u\end{bmatrix}\quad \mathbf{q}_{(T)}=\begin{bmatrix}q\\ \alpha\\ \psi\end{bmatrix}.$$

Then (see Fig. 1), with $\alpha=(\mathbf{E},\mathbf{q})=(\mathbf{z},\mathbf{z}')=(\mathbf{x},\mathbf{x}')$,

$$\mathbf{k}=(k\sin\xi\cos u)\mathbf{x}'+(k\sin\xi\sin u)\mathbf{y}'+(k\cos\xi)\mathbf{z}',$$

where

$$\mathbf{x}'=\mathbf{x}\cos\alpha-\mathbf{z}\sin\alpha;\quad \mathbf{y}'=\mathbf{y};\quad \mathbf{z}'=\mathbf{x}\sin\alpha+\mathbf{z}\cos\alpha.$$

The identification of k_z gives

$$\cos\theta=\cos\xi\cos\alpha-\sin\xi\sin\alpha\cos u.$$

Therefore

$$\cos\theta_0=s_0\cos\alpha-(1-s_0^2)^{1/2}\sin\alpha\cos u. \tag{A21}$$

Finally, with $\theta_0=\theta_0(u)$ given by Eq. (A21), one gets

$$f(k,u,s_0)=f[k,\theta_0(u)]. \tag{A22}$$

Expression for $\hat{C}_{ph}$. Equation (A7) can be written as

$$\hat{C}_{\rm ph}N(\mathbf{q})=\frac{[N(\mathbf{q})+1]}{q^2}2C_{\rm po}\times\int_{u=0}^{2\pi}\int_{k=k_{\min C}}^{k_{\max}}\frac{G(k,q,s_0)f(k,u,s_0)}{|\partial H_c/\partial s|_{s=s_0}}\times k^2dk\,du. \tag{A23}$$

$k_{\min C}$ is given by Eqs. (A14), and $k_{\max}$ is chosen such that $f(k_{\max})$ is negligible.

The double integral (A23) has no analytical solution. The electron distribution function is tabulated at the k_i and θ_j values of the mesh in $\{\mathbf{k}\}$ space through the numerical solution of the electron Boltzmann equation. The first numerical integration of Eq. (14) is performed over u, from 0 to π instead of 0 to 2π, taking into account the symmetry of Eq. (19). Since Eq. (A19) shows that $|\partial H_c/\partial s|$ does not depend on u, Eq. (A23) can be written as

$$\hat{C}_{\rm ph}N(\mathbf{q})=2\frac{[N(\mathbf{q})+1]}{q^2}2C_{\rm po}\times\int_{k=k_{\min C}}^{k_{\max}}\frac{G(k,q,s_0)}{|\partial H_c/\partial s|_{s=s_0}}k^2dk\times\int_{u=0}^{\pi}f(k,u,s_0)du. \tag{A24}$$

This equation holds for $q_{\min}\le q\le q_{\max}$, where

$$q_{\min}=k(\varepsilon_{\max})-k(\varepsilon_{\max}-\hbar\omega_{\rm LO}),\qquad q_{\max}=k(\varepsilon_{\max})+k(\varepsilon_{\max}-\hbar\omega_{\rm LO}). \tag{A25}$$

In practice, this value $q_{\max}$ is very large; we limited ourselves to $q_{\max}=1.5\times10^9\ \mathrm{m}^{-1}$.

Finally, carrying into Eq. (A24) the results of Eqs. (12b), (12c), (A20), and (A19), one gets Eqs. (14), (15), (16), and (17) of Sec. III B.

APPENDIX B: MATERIAL PARAMETERS USED FOR InP

(Values for *X* valleys have not been used in the present work)

General characteristics:

Quantity	Symbol	Unit	Value
Mass density	ρ	g/cm^3	4.83
Sound velocity	s	m/s	5160
HF relative dielectric constant	ε_∞		9.56
Static relative dielectric constant	ε_r		12.3

Band parameters:

Quantity	Symbol	Unit	Valley Γ	Valley L	Valley X
Relative effective mass	m^*		0.08	0.4	0.4
Nonparabolicity factor	α^*	$(\text{eV})^{-1}$	0.627	0.621	0.204
Gap referred to Γ minimum	Δ	eV	0	0.610	0.80
Number of equivalent valleys	Z_{ij}		1	4	3

Intravalley scattering parameters:

Quantity	Symbol	Unit	Valley Γ	Valley L	Valley X
Acoustic deformation potential	E_{ac}	eV/m	7	12	11
Piezoelectric constant	P_{pi}	Cb/m^2	0.0131	0.0131	0.0131
TO phonons:					
Deformation potential		eV/m		6.7×10^{10}	
Energy	$\hbar\omega_{TO}$	meV		43	
LO phonons:					
Energy	$\hbar\omega_{LO}$	meV	43.20	43.20	43.20

Intervalley scattering parameters:

Intervalley phonon 1:

	Energy $\hbar\omega_{ij}$ (meV)				Deformation potential E_{ij} (10^9 eV/m)		
	Γ	L	X		Γ	L	X
Γ		33.7	33.7	Γ		137	125
L	33.7	33.7	33.7	L	137	56	84
X	33.7	33.7	23.9	X	125	84	99

Intervalley phonon 2:

	Energy $\hbar\omega_{ij}$ (meV)				Deformation potential E_{ij} (10^9 eV/m)		
	Γ	L	X		Γ	L	X
Γ		6.8	8.4	Γ		14	7.5
L	6.8		6.8	L	14		19.4
X	8.4	6.8	12.8	X	7.5	19.4	1.0×10^{-4}

APPENDIX C: EFFECT OF HOT PHONONS ON ELECTRONIC TRANSPORT PARAMETERS

Electrons in InP, $T=300$ K, $N_D=1\times10^{17}$ cm^{-3}

1. Transport parameters without taking into account hot phonons

The following results were obtained after solving the Boltzmann equations for the electrons in the Γ and in the L valleys with the parameters given in Appendix B for the electrons, assuming that the phonons are in thermal equilibrium.

Field E (kV/cm)	Velocity Γ valley (10^7 cm^{-1})	Velocity L valleys (10^7 cm^{-1})	Drift velocity (10^7 cm^{-1})	Energy Γ valley (meV)	Energy L valleys (meV)	Average energy (meV)	% electrons in L valleys
0.01	0.003 075	0	0.003 075	40.5	652.5	40.9	0.0624
1	0.281	0.0092	0.281	40.8	658	42.3	0.3
2	0.546	0.0182	0.543	44.3	657	47.4	0.5
5	1.25	0.0484	1.23	66	659	75.8	2
10	2.21	0.100	2.07	161	654	192	6
20	2.10	0.205	1.51	341	657	440	31
50	1.59	0.427	0.933	436	671	569	57

2. Transport parameters taking into account hot phonons

The following results were obtained after solving the coupled electron–LO-phonon Boltzmann equations, with the parameters given in Appendix B for the electrons, and with $\tau_0 = 16$ ps, yielding $\tau_L = 5.8$ ps at 300 K.

Field E (kV/cm)	Velocity Γ valley (10^7 cm^{-1})	Velocity L valleys (10^7 cm^{-1})	Drift velocity (10^7 cm^{-1})	Energy Γ valley (meV)	Energy L valleys (meV)	Average energy (meV)	% electrons in L valleys
0.01	0.004 234	0	0.004 234	40.6	652.5	40.9	0.10
1	0.402	0.001 40	0.402	45.8	666	45.8	0.17
2	0.769	0.002 87	0.769	47.7	666.8	47.6	0.30
5	1.51	0.062 2	1.500	86.2	668.7	91.8	1
10	2.16	0.121	1.91	237	667	289	11.9
20	1.988	0.207	1.34	375	668	482	36.4
50	1.64	0.424	0.933	460	681	589	58.2

[1] P. Kocevar, in *Physics of Nonlinear Transport in Semiconductors,* Vol. 52 of *NATO Advanced Study Institute,* edited by D. K. Ferry, J. R. Barker, and C. Jacoboni (Plenum, New York, 1980).

[2] V. L. Gurevich, *Transport in Phonon Systems* (North-Holland, Amsterdam, 1986).

[3] J. Shah, J. Phys. (Paris) Colloq. **42**, C7-445 (1981).

[4] R. Ulbrich, J. Phys. (Paris) Colloq. **42**, C7-423 (1981).

[5] J. Shah, R. C. C. Leite, and J. F. Scott, Solid State Commun. **8**, 1089 (1970).

[6] P. Kocevar, J. Phys. C **5**, 3349 (1972).

[7] M. Rieger, P. Kocevar, P. Lugli, P. Bordone, L. Reggiani, and S. Goodnick, Phys. Rev. B **39**, 7866 (1989).

[8] P. Kocevar, Adv. Solid State Phys. **27**, 197 (1987).

[9] J. P. Aubert, J. C. Vaissière, and J. P. Nougier, J. Appl. Phys. **56**, 1128 (1984).

[10] P. G. Klemens, Phys. Rev. **148**, 845 (1966).

[11] R. K. Chang, J. M. Ralston, D. E. Keating, *Proceedings of the International Conference on Scattering Spectra in Solids,* edited by C. B. Wright (Springer-Verlag, New York, 1969), p. 369.

[12] D. Von der Linde, J. Kuhl, and H. Klingenberg, Phys. Rev. Lett. **44**, 1505 (1980).

[13] A. Mooradian, in *Laser Handbook,* edited by F. T. Arecchi and E. D. Schutz du Bois (North-Holland, Amsterdam, 1972), p. 1410.

[14] E. M. Conwell and M. O. Vassel, Phys. Rev. **166**, 797 (1968).

[15] M. L. Cohen and T. K. Bergstresser, Phys. Rev. **141**, 789 (1966).

[16] M. A. Littlejohn, J. R. Hauser, and Th. Glisson, J. Appl. Phys. **48**, 4587 (1977).

[17] B. R. Nag, *Electron Transport in Compound Semiconductors* (Springer-Verlag, New York, 1980).

[18] W. Fawcett, A. D. Boardman, and S. Swain, J. Phys. Chem. Solids **31**, 1963 (1970).

[19] E. G. S. Paige, Prog. Semicond. **8**, 62 (1964).

[20] J. Bardeen and W. Schockley, Phys. Rev. **80**, 72 (1950).

[21] C. Herring and E. Vogt, Phys. Rev. **101**, 944 (1956).

[22] E. M. Conwell, *High Field Transport in Semiconductors* (Academic, New York, 1967).

[23] B. R. Nag, Solid State Commun. **11**, 987 (1972).

[24] R. S. Crandall, Phys. Rev. B **1**, 730 (1970).

[25] W. A. Harrison, Phys. Rev. **104**, 1281 (1956).

[26] P. Lawaetz, Phys. Rev. **183**, 730 (1971).

[27] M. Lax and J. J. Hopfield, Phys. Rev. **104**, 128 (1956).

[28] H. W. Streitwolf, Phys. Status Solidi **37**, K47 (1970).

[29] H. Brooks, C. Herring, Phys. Rev. **83**, 879 (1951).

[30] H. Brooks, Adv. Electron. Electron. Phys. **7**, 85 (1955).

[31] B. K. Ridley, J. Phys. C **10**, 1589 (1977).

[32] T. C. Damen, R. C. C. Leite, and J. Shah, *Proceedings of the Tenth International Conference on the Physics of Semiconductors,* edited by S. P. Keller, J. C. Hensel, and F. Spern (U.S. Atomic Energy Commission, Cambridge, Massachusetts, 1970), p. 735.

[33] P. Kocevar, J. Phys. C **5**, 3349 (1972).

[34] W. Fawcett, A. D. Boardman, and S. Swain, J. Phys. Chem. Solids **31**, 1963 (1970).

[35] M. Fadel, Thèse de Doctorat ès Sciences, Université des Sciences et Techniques du Languedoc, Montpellier, France, 1988.

[36] W. Fawcett and D. C. Herbert, Electron. Lett. **9**, 308 (1973).

[37] G. H. Glover, Appl. Phys. Lett. **20**, 224 (1972).

[38] L. Drud Nielsen, Phys. Lett. **38A**, 221 (1972).